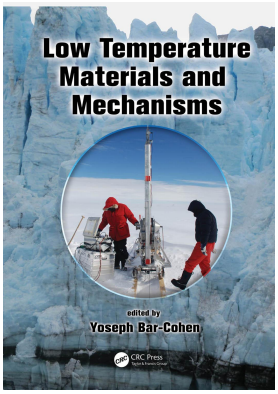

Low Temperature Materials and Mechanisms

Yoseph Bar-Cohen

Solids and Fluids at Low Temperatures

Publication details
https://www.routledgehandbooks.com/doi/10.1201/9781315371962-4
Yoseph Bar-Cohen
Published online on: 13 Jul 2016

3

Solids and Fluids at Low Temperatures

Steve Vance, Thomas Loerting, Josef Stern, Matt Kropf, Baptiste Journaux, Corey Jamieson, Morgan L. Cable, and Olivier Bollengier

CONTENTS

3.1 Introduction

The fundamental properties of low temperature materials have garnered greater interest with the advent of space exploration. Space technology must survive fluctuations and lows in temperature rarely encountered on Earth. Of deeper scientific interest and continuing mystery is the range of new thermodynamic properties and rheologies (e.g., elasticity, tensile strength, viscosity) of planetary materials encountered on the Moon and Mars, comets, and a multitude of icy worlds. Properties of industrial metals and plastics have been discussed in recent chapters published elsewhere [Van Sciver, 2012], including low temperature heat capacity, thermal contraction, electrical and thermal conductivity, magneto-resistance in metals, and solid–liquid phase changes [Mehling and Cabeza, 2008]. This chapter describes materials and their relevant properties, which we are just beginning to understand in the detail that future exploration requires. It ends with a brief note about applications of piezoelectric materials at low temperatures.

3.2 Solid Materials

At very low temperatures, water and other solid materials that are present on icy satellites have mechanical and chemical properties that resemble those of rocks and metals. This analogy makes them interesting as key to icy satellite geology, but also possibly as industrial materials.

The chemical and physical properties of a solid are greatly influenced by the conditions under which it was formed due to variations in the molecular arrangement. Solids may be *crystalline*, with ordered and repeating fundamental units at the molecular level. This generally gives rise to anisotropic physical properties, higher and sharply defined melting points, and higher thermal conductivities when compared to analog *amorphous* solids that do not have a long-range order [Eucken, 1911; Hendricks and Jefferson, 1933; Lonsdale, 1937]. The degree and type of crystallinity may depend on several factors including pressure, rate and temperature of freezing or deposition, thermal history, specific molecular makeup/existence of impurities, or the presence of bond-disrupting processes [Johannessen et al., 2007; Sestak et al., 2011]. The crystalline state is energetically favored, but kinetically driven formation processes may result in amorphous structures if the atoms do not have time to orderly arrange to the lower-energy crystalline state [Zallen, 1983]. If water is cooled at a rate greater than 10^6 K s^{-1}, the crystalline state does not have time to form and an amorphous solid is formed [Bruggeller and Mayer, 1980].

The geometry of crystalline solids of single repeating units can be classified by one of 14 symmetrically unique lattice structures, called *Bravais lattices*. However, much crystalline material, such as salts or molecular solids, is composed of multiple fundamental units, which break the symmetry of the 14 Bravais lattices and must be defined with additional symmetry elements. These elements are called *point groups*, and the combination of the Bravais lattices and the point groups leads to 230 potential *space groups* that provide the necessary symmetry elements to describe a 3D crystalline solid [Sands, 1975].

Substances often occur in several different crystalline phases—a phenomenon known as *polymorphism*—which depends on the conditions of formation. For example, on distant, frigid bodies of the outer solar system such as Pluto and Triton (a moon of Neptune), nitrogen ice can exist in two phases—a cubic α-phase or a hexagonal β-phase—with a transition temperature between them at 35.6 K. Their differing molecular structures change the electronic and vibrational environment of the material. The difference can be identified in spectroscopic analyses of the surface and has been used to elucidate the surface temperature of these bodies [Grundy et al., 1993; Quirico et al., 1999].

Polymorphism is one of water's anomalous properties: 17 distinct crystalline phases are known at present [Petrenko and Whitworth, 2002; Falenty et al., 2014], labeled by Roman numerals following the chronological order of their discovery. The first new phase (besides hexagonal I_h), described in 1900, was named ice II [Tammann, 1900]; the most recent one, ice XVI, was discovered in 2014 [Falenty et al., 2014]. Other phases may exist [e.g., Wilson et al., 2013; Algara-Siller et al., 2015].

Specific crystal or amorphous structures are identified by analyzing the glass transition temperature or associated thermodynamic quantities; x-ray scattering or electron diffraction patterns; or NMR splitting pattern to determine bond correlation [Stachurski, 2011].

The process of crystallization can be understood as the balance between the enthalpic benefit of bond formation and the entropic drive to disorder. Upon cooling, the kinetic energy of molecules and atoms decreases, diminishing the thermodynamic contribution of entropy. At low temperatures, when the Gibbs free energy is enthalpically dominated,

solidification becomes thermodynamically spontaneous. However, not every thermodynamically favored cooling process immediately results in solidification. Even if the phase transformation of the bulk sample is considered spontaneous, below a critical size the transformation of the molecular units may not be. Nucleation sites, if present, often enable crystal formation by allowing additional transitions to take place [De Yoreo and Vekilov, 2003]. If nucleation sites do not exist, liquids may be cooled below the thermodynamically determined solid–liquid phase boundary—a condition known as *supercooling*. For example, water normally freezes at 273 K at 1 atmosphere of pressure, but can be supercooled at the time scale of milliseconds down to 232 K while remaining liquid [Sellberg, 2014].

3.2.1 Crystalline Ices

The phase diagram shown in Figure 3.1 depicts the stability fields of liquid and solid phases of water. That is, the phase diagram merely shows the one phase that is thermodynamically most stable at a specific combination of pressure P and temperature T. Some ice phases, namely ices IV, IX, XII, XIII, XIV, and XVI, cannot be found in Figure 3.1 because they are never the thermodynamically most stable phase. In spite of this metastable nature, such phases readily form and can be isolated and characterized. They do not convert to more stable ice phases at laboratory time scales, and probably also not at astrophysically relevant time scales, provided the temperature and pressure conditions do not change. Crystalline phases can be stable in a P–T field or metastable at all P–T conditions. Some stable ice phases share a phase boundary with liquid water (ices I_h, III, V, VI [e.g., Choukroun and Grasset, 2007 and references therein] and ice VII [Pistorius et al., 1963; Mishima and Endo, 1978; Datchi

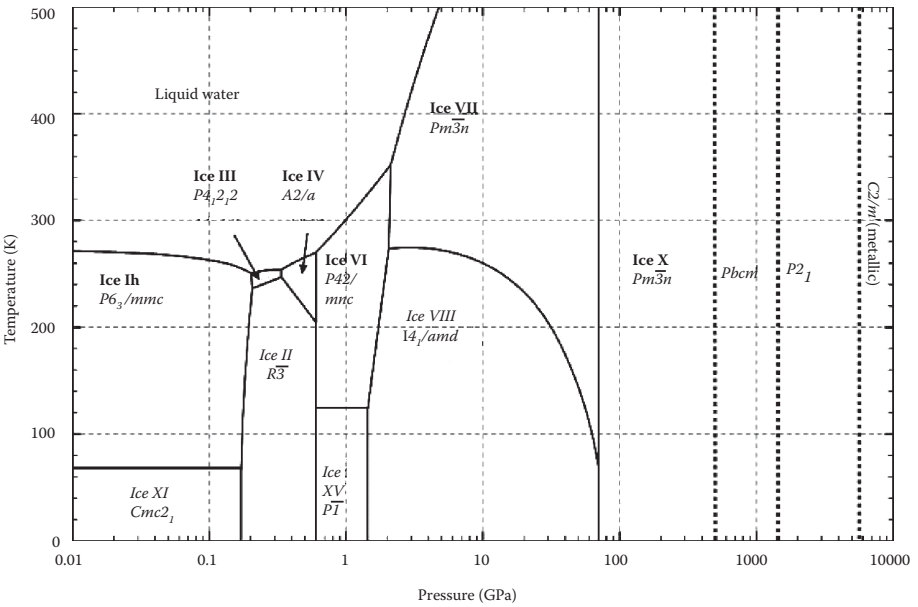

FIGURE 3.1
Phase diagram of H_2O from 0.01 to 10000 GPa and 0 to 500 K, showing stable water phases and their space group when crystalline. Proton disordered phases are written in bold, and proton-ordered phases are written in italics. Phase boundaries are plotted with a thick black line and predicted phase boundaries predicted at ultra-high pressures using computational simulations in dotted lines. (Courtesy of Baptiste Journaux, coauthor of this chapter.)

et al., 2000]), and are disordered [Kuhs, 2007]. Other ice phases are proton ordered and only exist in thermodynamic equilibrium with other ice polymorphs, namely ices II [Kamb, 1964; Kamb et al., 1971; Arnold et al., 1968; Fortes et al., 2003, 2005], VIII [Whalley et al., 1966; Kuhset al., 1984; Jorgensen et al., 1984, 1985; Pruzan et al., 1990, 1992; Besson et al., 1994, 1997; Pruzan et al., 2003; Song et al., 2003; Singer et al., 2005; Knight et al., 2006; Yoshimura et al., 2006; Somayazulu et al., 2008; Fan et al., 2010], XI [Singer et al., 2005; Knight et al., 2006; Fan et al., 2010; Tajima et al., 1984; Matsuo et al., 1986; Fukazawa et al., 1998, 2002; Kuo et al., 2005], XII [Kuhs et al., 1998; Lobban et al., 2000; Salzmann et al., 2006a, 2006b, 2008; Knight and Singer, 2008], XIV [Salzmann et al., 2006a, 2006b; Tribello et al., 2006], and XV [Kuhs et al., 1984; Fan et al., 2010; Knight and Singer,2005; Kuo and Kuhs, 2006; Salzmann et al., 2009]. Such high-pressure ice phases may be found in the mantles of the icy moons, for example, Ganymede, which is covered by an 800-km-thick layer of water ice [Vance et al., 2014], as well as Callisto [Schubert et al., 2004] and Titan [Tobie et al., 2005; Fortes et al., 2007] (Figure 3.2). It is also expected that high-pressure ices play a key role in ocean planets [Leger et al., 2004; Sotin et al., 2007; Grasset et al., 2009], roughly Earth-sized exoplanets with deep oceans that constitute an interesting analog to the icy satellites (Figure 3.2).

The distinction between proton-ordered and proton-disordered ice phases is shown in Figure 3.3. In all ice phases, the oxygen atoms occupy lattice positions, that is, the oxygen atoms are ordered over long ranges. The hydrogen atoms occupy lattice positions only in

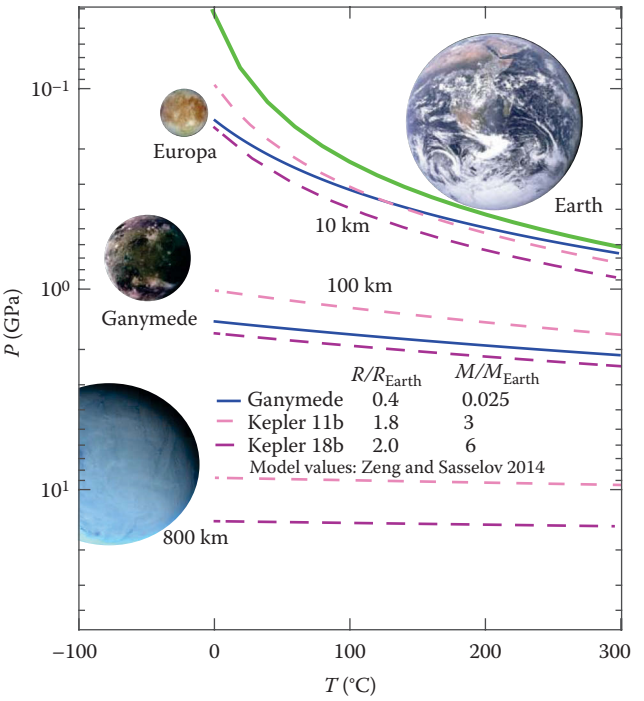

FIGURE 3.2
Pressures in exoplanet oceans span the multi-GPa range of pressures where liquids are possible. A Europa-depth ocean on Earth would behave like Ganymede's ocean in terms of having high-pressure ices. This figure shows profiles of pressure (GPa) and temperature (°C) in the upper mantles of selected objects (modified from Vance, S. et al., *Astrobiology*, 7(6), 2007), beginning at the estimated depth of the seafloor. The overlying ocean is assumed to be at a constant temperature; in general, seafloor temperature will be elevated by more than 40°C in deep oceans. Known exoplanets, albeit very hot ones, are modeled as super Europa objects with seafloor depths like Earth's (10 km), Europa's (100 km), and Ganymede's (800 km). (Courtesy of Steve Vance, principal author of this chapter.)

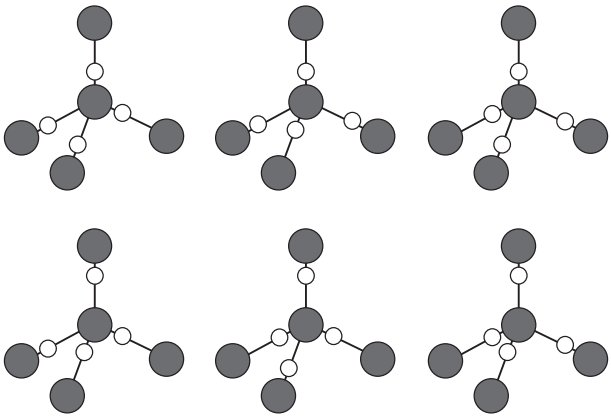

FIGURE 3.3
Six different proton configurations (white circles) allowed by the Bernal–Fowler ice rules. In proton-ordered ices, only one of these is observed, whereas in proton-disordered ices, all of these configurations are observed with equal probability. The tetrahedral coordination around a central oxygen atom (filled circles) is the motif found in all crystalline and amorphous ices (except for the ultrahigh-pressure phases at >100 GPa, ice X and the post-ice X phases). (Adapted from Fuentes-Landete, V., *Proceedings of the International School of Physics "Enrico Fermi," Volume 187: Water: Fundamentals as the Basis for Understanding the Environment and Promoting Technology*, IOS and Bologna: SIF, Amsterdam, 2015.)

the case of the proton-ordered ice phases. For a given network of oxygen atoms, in principle a larger number of ordered proton configurations are possible. Experimentally, however, only a single type of ordering has been observed so far. Ice I_h, the most common form of ice on Earth, is a proton-disordered form of ice. The hydrogen atoms obey the Bernal–Fowler ice rules [Bernal and Fowler, 1933], but they are randomly distributed within the ice crystal. As a result, ice I_h represents a frustrated crystal, which does not have zero configurational entropy at 0 K. The residual entropy at 0 K has become famous as the Pauling entropy ΔS_P [Pauling, 1935] and amounts to approximately 3.41 J K^{-1} mol^{-1}. This entropy can be released if one successfully achieves the transformation to the proton-ordered state. The ordered counterpart of ice I_h is known as ice XI, and its possible ferroelectric nature is currently being questioned [Parkkinen et al., 2014]. Order–disorder pairs can be easily recognized in the phase diagram in Figure 3.1 because the pair is separated by a phase boundary parallel to the pressure axis. This is so because there is barely any volume difference between proton-ordered and proton-disordered form, that is, $\Delta V \approx 0$, but the two ices differ by the Pauling entropy, that is, $\Delta S \approx \Delta S_P$. The slope of the phase boundary dP/dT then goes to infinity, that is, parallel to pressure axis, according to the Clausius–Clapeyron equation $dP/dT = \Delta S/\Delta V$.

Solid–solid transitions between polymorphs are possible by either a rearrangement of the O-lattice (density-driven, e.g., by pressurization) or H-ordering/disordering while preserving the geometry of the O-atoms (entropy-driven, e.g., by cooling a disordered phase to form an ordered one). In the case of density-driven transitions, there is a finite volume change ΔV, but the entropy change may be close to zero $\Delta S \approx 0$ if the transition is from a proton-disordered to a proton-disordered phase. Such phase boundaries can be identified easily in Figure 3.1, since they are almost parallel to the temperature axis. With increasing pressure, the transition sequence $I_h \rightarrow III \rightarrow V \rightarrow VI \rightarrow VII \rightarrow X$ can be identified. All these ice phases, except for ice X, are proton-disordered and of increasing density, starting at 0.92 g cm^{-3} and ending at 2.50 g cm^{-3}. High density is accommodated by improving packing, bending hydrogen bonds, and forming new hydrogen-network topologies. The oxygen networks differ in terms of topology and ring structure. While ices I_h and I_c consist entirely of six rings, ice V

has 4-, 5-, 6-, 8-, 9-, 10-, and 12-ring structures [Herrero and Ramírez, 2013]. Some structures show ring threading; for example, ice IV and others show two interpenetrating ice networks (self-clathrates), for example, ices VI, VII, VIII, and X. For the latter ultrahigh-pressure ice X (>100 GPa [Benoit et al., 1996; Pruzan et al., 2003]), the molecular nature disappears due to the symmetrization of hydrogen position between the oxygen atoms.

Three low-density variants of crystalline ice can be produced at ambient pressure: hexagonal ice I_h, cubic ice I_c, and ice XI. While ice I_h is the abundant polymorph of solid H_2O on Earth, ice I_c can occasionally be found in clouds [Murray et al., 2005; Mayer and Hallbrucker, 1987; Whalley, 1983]. Ice I_c forms upon heating of amorphous ice in a vacuum or at ambient pressure. It may thus be present on comets after they have experienced temperatures above the crystallization temperature of ~150 K. It also forms upon heating of high-pressure forms of ice at/below ambient pressure and upon condensation of water vapor on particles at ~140–200 K. Both are very similar in density at P_{atm}, also appearing to be identical when probing the short-range molecular environment (e.g., Raman or mid-infrared). However, they can be distinguished when examining the long-range order (e.g., x-ray diffraction or neutron diffraction) [Kuhs et al., 1987]. Ices I_h and I_c are polytypical relative to each other: identical layers—differing stacking order (hexagonal rings, ABCABC with hexagonal symmetry for I_h, ABAB with fcc symmetry for I_c) [Kuhs and Lehmann, 1986; Kuhs et al., 1987; Guinier et al., 1984; Röttger et al., 1994]. I_c is not obtained as a single crystal, but only in the form of small crystallites with roughly hexagonal stacking faults (quantified by "cubicity index") [Kuhs et al., 1987; Kohl et al., 2000; Hansen et al., 2007]. Ice XI, the proton-ordered form of ice I_h, is only stable at $T < 72$ K. A proton-ordered form of cubic ice I_c might also exist, as has been suggested by *in situ* IR experiments and *ab initio* simulations [Geiger et al., 2014].

As mentioned, a crystalline phase may be transformed into another by ordering/disordering the protons while almost entirely preserving the O-atom topology. These order–disorder pairs will be found in the same P region of the phase diagram (I_h–XI [Singer et al., 2005; Knight et al., 2006; Fan et al., 2010; Tajima et al., 1984; Matsuo et al., 1986; Fukazawa et al., 1998, 2002; Kuo et al., 2005], III–IX [Fan et al., 2010; Kuhs et al., 1998; Lobban et al., 2000; Whalley et al., 1968; LaPlaca et al., 1973; Nishibata and Whalley, 1974; Minceva-Sukarova et al., 1984; Londono et al., 1993; Knight et al., 2006], V–XIII [Kuhs et al., 1998; Lobban et al., 2000; Salzmann et al., 2006a, 2008; Knight et al., 2008; Martin-Conde et al., 2006; Noya et al., 2008], VI–XV [Kuhs et al., 1984; Fan, 2010; Knight and Singer, 2005; Kuo and Kuhs, 2006; Salzmann et al., 2009], VII–VIII [Whalley et al., 1966; Kuhs et al., 1984; Jorgensen et al., 1984, 1985; Pruzan et al., 1990, 1992, 2003; Besson et al., 1994, 1997; Song et al., 2003; Singer et al., 2005; Knight et al., 2006; Yoshimura et al., 2006; Somayazulu et al., 2008; Fan et al., 2010], and XII–XIV [Salzmann et al., 2006a, 2006c; Tribello et al., 2006; Martin-Conde et al., 2006; Noya et al., 2008; Köster et al., 2015]), the ordered phase at lower and the disordered phase at higher temperatures (as the transition connected to the process of disordering an ordered phase is of entropic nature). Six configurations are allowed by the Bernal–Fowler ice rules in the local tetrahedral hydrogen-bond geometry known as Walrafen pentamer. In a fully disordered phase, all six are populated with the same probability (averaged over space/time) [Bernal and Fowler, 1933], whereas in an ordered phase, only one configuration is found. Often, the ordered low temperature phase cannot be accessed due to geometric constraints and kinetic limitations at such low temperatures. Point defects (Bjerrum L/D or ionic defects) in the ice lattice may enhance the reorientational mobility in the ice lattice. By using dopants incorporated into the ice lattice in ice I_h (e.g., HCl, HBr, HF, NH_3, KOH, etc. [Tajima et al., 1984; Matsuo et al., 1986; Hobbs, 1974; Gross and Svec, 1997]) and also at a higher pressure in ice VII (e.g., NaCl, LiCl, RbI [Frank et al., 2006, 2013; Klotz et al., 2009; Journaux et al., 2015]), such point defects may be introduced deliberately. These extrinsic defects may enhance the mobility

related to rearrangement of protons and/or rotation of H_2O molecules, thereby overcoming kinetic limitations and allowing access to the proton-ordered low temperature phase [Köster et al., 2015]. However, this may also slow down the dynamics. Empirically it has been found that KOH doping accelerates dynamics in ice I_h whereas HCl doping has been found to accelerate the dynamics in the high-pressure ices V, VI, and XII [Salzmann et al., 2006a, 2006b, 2009]. The reasons why one dopant is effective and the other is not are still unclear, but are certainly related to the dynamics of pairs of point defects within the ice lattices [Burton and Oliver 1935; Mayer and Pletzer 1986]. Some ice phases do not form an order–disorder pair; new ice phases related to them through an order–disorder transition may be found in the future. For example, the ordered counterparts of I_c and IV, as well as the disordered one of II, still await discovery [Lokotosh and Malomuzh, 1993; Zabrodsky and Lokotosh, 1993].

The solubility of dopants in ice is generally assumed to be low. Ice I_h tends to reject any impurities during freezing [Gross and Svec, 1997]. For concentrated solutions, for example, freezing aqueous solutions present during sea ice formation, rejected salts may be incorporated in the bulk ice sheet at the grain boundaries as liquid brine inclusions [Weeks and Akley, 1986]. For the H_2O–NaCl system, the partition coefficient K_d (NaCl) is estimated around 2.7×10^{-3} and $3.2\ (\pm 0.2) \times 10^{-3}$ [Gross et al., 1977, 1987]. This incompatible behavior of salts in ice I_h has a notable exception with ammonium fluoride, which forms a solid solution by substituting with H_2O molecules up to 5.2 mol% [Gross and Svec, 1997], most likely due to the isomorphism between the crystal lattices of NH_4F and ice I_h. Such incorporation should be distinguished from that occurring in clathrate hydrates as the ice solid solution keeps the crystallographic structure of the pure H_2O phase. While most substances are completely insoluble in ice, some dopants can be incorporated in the ice crystal by replacing water molecules. In cases of HCl, KOH, NH_3, HBr, or HF, the solubilities are in the ppb and ppm range. In spite of the low solubility, the influence on H-dynamics can be huge.

Recent high-pressure experiments have shown that ice VII can incorporate up to 1.6 mol% of NaCl, 5 mol% of CH_3OH [Frank et al., 2006, 2013], and up to 16.7 mol% of LiCl [Klotz et al., 2009]. Using DFT *ab initio* calculations, Klotz et al. [2009] predict incorporation in ice VII at interstitial (face-centered) and lattice sites (H_2O substitution) for Li^+ and Cl^-, respectively (Figure 3.4). The presence of 16.7 mol% of Li^+ and Cl^- solutes in the ice VII cubic P*n*-*3m* lattice increases the volume of the phase by 8%, increasing the density by 0.2 g cm^{-3}. At low temperatures, the presence of Li and Cl ions inhibits the transition to proton-ordered ice VIII down to 80 K. Strong electrostatic interactions between the incorporated ions and the polar water molecules seem to disadvantage long-range ordering of the H_2O orientations,

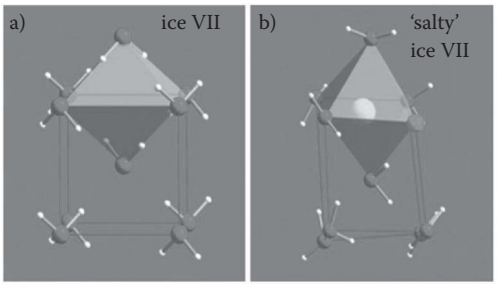

FIGURE 3.4
(a) Proton-disordered ice VII crystallographic structure in one possible proton configuration with the octahedral interstitial face-centered void. (b) Snapshot of a possible configuration of "salty" ice VII ($LiCl{\cdot}6H_2O$) derived from *ab initio* calculations illustrating the lattice distortion and H_2O misorientation induced by the incorporation of Li^+ (large circle) and Cl^- (medium circle) ions. (Modified from Klotz, S., *Nat. Mater.*, 8, 2009.)

as it may generate "crystal plasticity"* even at very low temperature. At present, the effect of neutral solutes on the transition to a proton-ordered phase remains unknown.

Incorporating substantial amounts of ionic and molecular solutes may affect the conductivity, volume, density, and thermodynamic stability of water ice. Such modifications of the physical properties of the solid are of interest for planetary scientists, as large water-rich planetary bodies may contain high-pressure ice mantles with thicknesses of hundreds of kilometers. As far as we know, no studies exist of solutes incorporated into other high-pressure ice phases of interest for icy moons and large H_2O-rich planets (e.g., ice III, V, VI, and X).

In the negative pressure regime, phases resembling the geometries of naturally occurring, cage-like clathrate structures are predicted to be thermodynamically stable [Stevenson et al., 1999]. Experiments have not yet been possible on ice at negative pressures. However, one empty clathrate structure could be prepared experimentally and is now known as ice XVI [Kuhs et al., 2014].

At ultrahigh pressures exceeding a few Mbar, currently not accessible experimentally, simulations predict new phases of ice [Wang et al., 2011; Militzer and Wilson, 2010; Hermann et al., 2012; Umemoto and Wentzcovitch, 2011; Sanloup et al., 2013].

3.2.2 Amorphous Ices

Just as polymorphism is regarded to be one of H_2O's anomalous properties, so is polyamorphism: the existence of more than one amorphous solid phase [Mishima et al., 1984, 1985].

One of solid water's amorphous low-density variants, most likely the most abundant form of water in the universe (amorphous solid water, ASW), is produced by the deposition of gaseous water or chemical reaction of atomic H, O, and OH on a very cold solid substrate. Experimentally ASW was produced by deposition of $H_2O_{(g)}$ on a cooled copper rod in early experiments [Ioppolo et al., 2010]. ASW naturally occurs on comets, satellites, interstellar dust, and in cold dark star-forming clouds in space [Mayer and Pletzer, 1986; Ehrenfreund et al., 2003; Ioppolo et al., 2010]). Depending on the conditions of formation (e.g., the temperature and general character of the substrate or the flow rates of the deposit gases [Stevenson et al., 1999; Cartwright et al., 2008; Bossa et al., 2012], the produced ASW may be highly microporous, resulting in specific surface areas of several hundred and even more than 1000 m^2/g [Baragiola, 2003]. These micropores will collapse when temperatures are raised, forming a much more compact variant of ASW with a specific surface area of less than 1 m^2/g [Baragiola, 2003; Mitterdorfer, 2014]. During formation of microporous noncollapsed ASW and in the presence of trace gases (e.g., in the cold regions of dense interstellar clouds), gas molecules can be trapped inside the pores [Ehrenfreund et al., 2003; Mitterdorfer et al., 2011]. Chemical reactions of trapped molecules in the micropores are promoted, and ASW may thus play a pivotal role in the very early stages of planet building [Ehrenfreund et al., 2003]. Furthermore, when pore collapse is induced while guest molecules are trapped, clathrate hydrates may form as a result [Mitterdorfer et al., 2011; Faizullin et al., 2014].

As shown in Figure 3.5, low-density forms of amorphous $H_2O_{(s)}$ are experimentally obtainable in three ways: cryo-deposition of gaseous H_2O (ASW) [Burton and Oliver, 1935], cryo-deposition of micrometer-sized droplets (also on a cooled substrate; hyper-quenched glassy water, HGW) [Mayer, 1985; Kohl et al., 2005] and decompression of higher-density forms of amorphous solid water at elevated temperatures (low-density amorphous ice, LDA) [Mishima et al., 1985]. All of them behave like glassy solids and seem to transform to a deeply supercooled, ultraviscous liquid upon heating, which is known as low-density

* Molecular crystal with dynamical disorder in the orientation of its constituent molecules, in which flip rates range from picoseconds to nanoseconds.

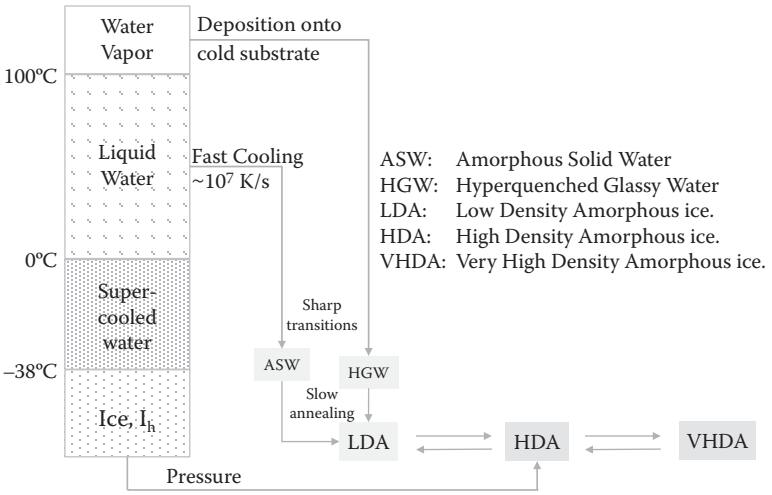

FIGURE 3.5
Preparation routes for amorphous ices, starting from water vapor (leading to ASW), from liquid water (leading to HGW) and from crystalline ice (leading to HDA). Note that the acronyms ASW, HGW, and LDA represent the same structural state (commonly called "LDA") after annealing at >110 K for a few minutes. This is indicated by the dashed arrows. The three polyamorphic forms LDA, HDA, and VHDA can reversibly be interconverted by compression/decompression experiments. (Modified from Fuentes-Landete, V., *Proceedings of the International School of Physics "Enrico Fermi," Volume 187: Water: Fundamentals as the Basis for Understanding the Environment and Promoting Technology*, IOS and Bologna: SIF, Amsterdam, 2015.)

liquid (LDL) water. The temperature of this transformation, known as glass-to-liquid transition, depends on the heating rate, found to be 124 K for slow heating (10 K/h) [Handa et al., 1986], 136 K for "common" heating (10 K/min), and 170 K for very fast heating rates (10^5 K/s) [Sepúlveda et al., 2012]. ASW/HGW/LDA have been shown by DSC at "common" rates to exhibit very similar glass transition temperatures (T_g) of 136–137 K [Hallbrucker et al., 1989; Johari et al., 1987; Elsaesser et al., 2010]. Mechanical indentation experiments have indicated softening and penetration of the material at about 143 K [Johari, 1998].

To date, two higher-density amorphous solid phases are known: high-density amorphous ice (HDA) and very high-density amorphous ice (VHDA), with sub-states of HDA differing in the degree of structural relaxation (unannealed HDA = uHDA [Mishima et al., 1984; Nelmes et al., 2006], expanded HDA = eHDA [Winkel et al., 2008; Salzmann et al., 2006d], and relaxed HDA = rHDA [Salzmann et al., 2006d]). HDA (uHDA) was the first high-density amorphous ice to be produced (in 1984) by compressing I_h to $P > 1$ GPa at 77 K [Mishima et al., 1984] (see Figure 3.5). VHDA can be formed by heating uHDA to temperatures below crystallization at pressures >0.8 GPa [Loerting et al., 2011]. eHDA behaves like a glassy solid and transforms upon heating into a deeply supercooled ultraviscous liquid—HDL water. The glass-to-liquid transition temperature was determined to be 116 K (10 K/min) at ambient pressure [Amann-Winkel et al., 2013].

Isotope substitution neutron diffraction experiments have shown ASW/HGW/LDA to be of highly similar structure [Bowron et al., 2006], as is also the case for uHDA–eHDA [Loerting et al., 2011]. However, uHDA and eHDA differ in their thermal stability (connected to their intrinsic states of relaxation), with uHDA transforming to LDA at approximately 110 K and eHDA at about 132 K at ambient pressure [Winkel et al., 2011].

However, the general question of whether HDA may be considered glassy (or possibly rather an assembly of nanoscaled polycrystallites) has remained [Loerting et al., 2009].

Studies have shown uHDA to first relax and then transform to LDA at P_{atm} [Handa et al., 1986]. At 1 GPa however, there appears to be a reversible glass–liquid transition at about 140 K [Andersson, 2011]. High-pressure experiments have presented dielectric relaxation times of VHDA of 100 s as early as 122 K at 1 GPa [Andersson, 2006]. Dilatometric analysis in the range of 0.1–0.3 GPa has located the onsets of reversible volume changes (attributed to possible glass transitions) to be between 134 and 142 K (at 0.1 and 0.3 GPa, respectively) [Seidl et al., 2011]. DSC measurements on eHDA at P_{atm} have indicated an onset of a glass transition at 116 K, presented as an endothermic feature that could not be found in the case of uHDA [Amann-Winkel et al., 2013]. All these findings suggest transformation of amorphous ices to ultraviscous, deeply supercooled liquids prior to crystallization at <160 K. At 140 K and 0.07 GPa, experimental evidence for spontaneous liquid–liquid phase separation and the formation of an interface between two ultraviscous liquids differing by 25% in density was obtained [Winkel et al., 2011]. At higher temperatures, these deeply supercooled liquids crystallize inevitably and rapidly, and so the thermodynamic connection between amorphous ices/deeply supercooled water and stable/supercooled water above 230 K remains unclear. At astrophysical time scales, water between about 160 and 240 K will always be crystalline.

3.2.3 Rheological Considerations

Durham and Stern [2001] reviewed the rheological properties of water ices, which influence planetary geology, including tectonics, crater formation and relaxation, and global thermal evolution.

Other low temperature materials produce frozen volatiles that are thought to be abundant on icy satellites and hypothesized exoplanets. Ammonia has been identified as a likely constituent in icy bodies beyond Jupiter, which implies a lower ice temperature and a strongly temperature-dependent viscosity [Croft et al., 1988; Durham et al., 1993; Arakawa and Maeno, 1994; Hogenboom et al., 1997; Leliwa-Kopystynski et al., 2002; Fortes et al., 2003]. The thermal conductivity of ammonia-rich (10%–30%) ice is two to three times lower than that of pure water ice, and the loss tangent is about 100 times greater [Lorenz and Shandera, 2001]. Intrinsic absorption in the ice matrix might be responsible for the latter. A recent study of the rheology of ammonia-water slurries as a function of temperature and strain rate show the development of yield stress-like behaviors, shear-rate dependence, and thixotropic behavior, even at relatively low crystal fractions [Carey et al., 2015]. Light and heavy alkanes familiar to the petroleum industry cover the surface of Titan and populate its atmosphere. Formation of methane and ethane clathrates may play a critical role in the evolution of Titan's atmosphere [Choukroun et al., 2010]. Such work has implications for icy satellites where cryovolcanism may exist, such as Triton and Titan.

Rheologies of other frozen volatiles have been studied in connection with other planets and a few locations on Earth: methane clathrate [Stern et al., 1996; Durham et al., 2003], CO2 [Durham et al., 1999], and N2 and CH4 [reviewed by Eluszkiewicz and Stevenson 1990]. Both brittle and ductile behaviors were observed for solid nitrogen and methane; the maximum strengths were determined to be 9 and 10 MPa, respectively, in the brittle failure mode [Yamashita et al., 2010]. These low strengths suggest that H_2O ice or other stronger materials may underlay solid N_2 and CH_4 to generate the topography observed on Triton.

The interaction of materials with different rheologies, melting points, and mixing behaviors has led planetary scientists to consider cryovolcanism as a class of geological process not found on Earth (Figure 3.6) [e.g., Kargel, 1994; Gaidos, 2001; Fagents, 2003; Sotin et al., 2005; Porco et al., 2006; Fortes et al., 2007; Desch et al., 2009; Cooper et al., 2009].

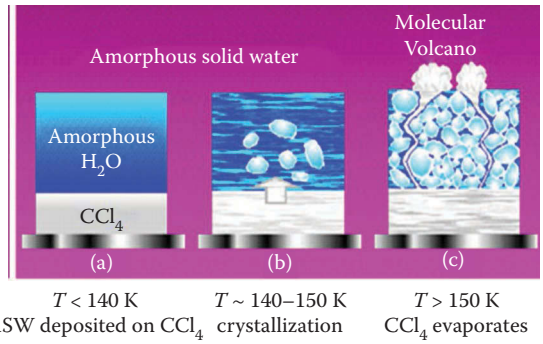

FIGURE 3.6
Amorphous solid water at various low temperatures. (Courtesy of AIP. With permission.)

3.3 Liquid Materials at Low Temperatures

Low temperature liquids are of interest for industrial and laboratory applications, and they exist in a surprising number of places throughout the solar system. Estimates of the thermal evolution of small icy planetary objects in the solar system indicate that natural radiogenic heating of their interiors alone would lead to internal liquid water oceans lasting millions of years [Hussmann et al., 2006]. Temperatures in the young outer solar system beyond Jupiter were below the freezing temperature of volatile species such as alkanes and ammonia, so these would have been included in distant worlds such as Pluto.

3.3.1 Structure of Liquids

Low temperature liquids display a range of viscosity, density, and thermal expansion. These properties determine the efficiency of thermal and material transport of extraterrestrial oceans [e.g., Vance and Goodman 2009; Vance et al., 2014].

Related to the existence of more than one amorphous phase of solid water is the hypothesis of there being more than one liquid phase of water in the supercooled region [Finney et al., 2002]. The liquid phases would be thermodynamically continuously connected to the amorphous solid phases and would correspondingly be of different density (LDL and HDL). At about 0.2 GPa, these two liquids may exist in thermodynamic equilibrium, that is, with a sharp interface between the two liquids of pure H_2O. So, the one-component system water at ambient conditions might in fact be a fluctuating mixture of two liquids, which may separate under low temperature and high pressure conditions. This, in turn, may indicate the possibility of a second critical point in the regime of these two different liquid phases [Stanley et al., 2000]. This second critical point cannot be accessed experimentally because of fast crystallization at its predicted location, and so has remained a virtual point up to now.

3.3.2 Properties of Water and Aqueous Systems

Aqueous solutions are stable in liquid form at an elevated pressure (250 MPa) to temperatures as low as 160 K [Mishima, 2011]. In the pure phase, liquid water exhibits ordering behavior that causes a maximum density at 4°C anomalous to the behavior of other simple fluids (Figure 3.7). The anomalous nature of water becomes more pronounced in

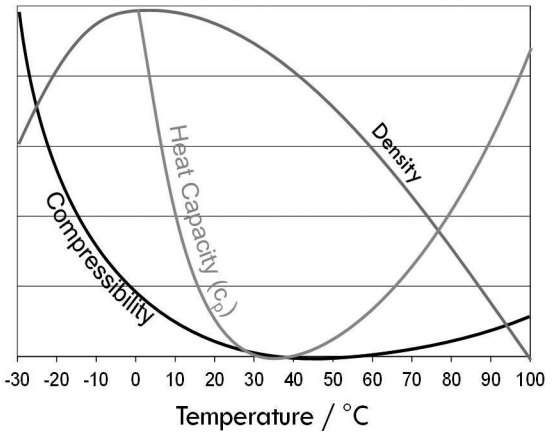

FIGURE 3.7
Compressibility, heat capacity, and density versus temperature. (Adapted from http://www.lsbu.ac.uk/water/.)

the supercooled state below 0°C. Response functions such as heat capacity or isothermal compressibility show a power-law increase, where a singular temperature of about 228 K was identified [Speedy and Angell, 1976]. These anomalies can be rationalized if the single-component system water experiences a spontaneous liquid–liquid separation into a HDL and LDL [Debenedetti, 2003]. The occurrence of polyamorphism (see Section 3.2.2) and the experimental evidence for spontaneous phase separation at 140 K and 0.07 GPa into the two ultraviscous liquids LDL and HDL [Winkel et al., 2011] support this theory. In the presence of sufficient amounts of solutes, the anomalies of water disappear and concentrated aqueous solutions behave as simple liquids.

Low temperature eutectic brines, the last occurring phase in freezing aqueous systems, represent a likely ocean composition in the ice-covered worlds [e.g., Zolotov and Kargel, 2009]. The array of possible compositions comprises a multicomponent space of low temperature liquids that requires a systematic and extensible representation of possible thermodynamic states. Such a systematic framework for computing thermodynamics of aqueous systems has been available for decades, based on the theoretical formulation of Kenneth Pitzer [1991]. The FREZCHEM implementation of the Pitzer thermodynamic framework (e.g., Marion et al., 2012) balances the activity of water (excess chemical potential) of aqueous solutions to compute the properties of aqueous systems in the presence of ice I. The underlying Gibbs energy is computed as the sum of contributions from dissolved cations (*c*) and anions (*a*), with pressure- and temperature-dependent coefficients describing the cation–anion interactions (B_{ca} and C_{ca}). Higher-order interactions become relevant for higher concentrations.

$$\frac{G^{ex}}{w_w RT} = f(I) + 2\sum_c\sum_a m_c m_a \left[B_{ca} + \left(\sum_c m_c z_c \right) C_{ca} \right]$$

$$+ \sum_{c<c'}\sum m_c m_{c'} \left[2\Phi_{cc'} + \sum_a m_a \psi_{cc'a} \right] + \sum_{a<a'}\sum m_a m_{a'} \left[2\Phi_{aa'} + \sum_c m_c \psi_{caa'} \right]$$

$$+ 2\sum_a\sum_c m_a m_c \lambda_{ac} + 2\sum_n\sum_a m_n m_a \lambda_{na} + 2\sum_{n<n'}\sum m_n m_{n'} \lambda_{nn'} + \sum_n m_n^2 \lambda_{nn} + \cdots$$

The Pitzer framework is useful for representing the multicomponent thermodynamics of water, but limited in its application to other worlds by Earth-centric data sets as illustrated by available density measurements for $MgSO_4$ shown in Figure 3.8.

Sound speed and specific heat capacity measurements in solutions at low temperature provide a sensitive probe of thermodynamic behaviors. Both are related to Gibbs free energy through the second derivatives in pressure and temperature, respectively:

$$\left(\frac{\partial \rho}{\partial P}\right)_{T,m} = \frac{1}{c^2} + \frac{T\alpha^2}{C_P}$$

$$\left(\frac{\partial C_P}{\partial P}\right)_{T,m} = -T\frac{\partial^2 V}{\partial T^2}$$

$$V = \frac{m}{\rho} = \left(\frac{\partial G}{\partial P}\right)_{T,m}$$

$$C_P = -T\frac{\partial^2 G}{\partial T^2}$$

Sound speed measurements in water [Vance and Brown, 2010; Lin and Trusler, 2012] and aqueous solutions [Chen and Millero 1977; Chen et al., 1978; Millero et al., 1985; Vance and Brown 2013] and nonaqueous systems at low temperatures provide a sensitive measure of water's thermodynamic properties, which can be used to systematically predict the behavior of multicomponent systems in low temperature settings.

Developing large thermodynamic frameworks is made possible by modern computers that can solve large inverse problems associated with sparse multiproperty thermodynamic data sets [Lemmon et al., 2013] and forward problems associated with *ab initio* molecular dynamics calculations [e.g., Hassanali et al., 2011].

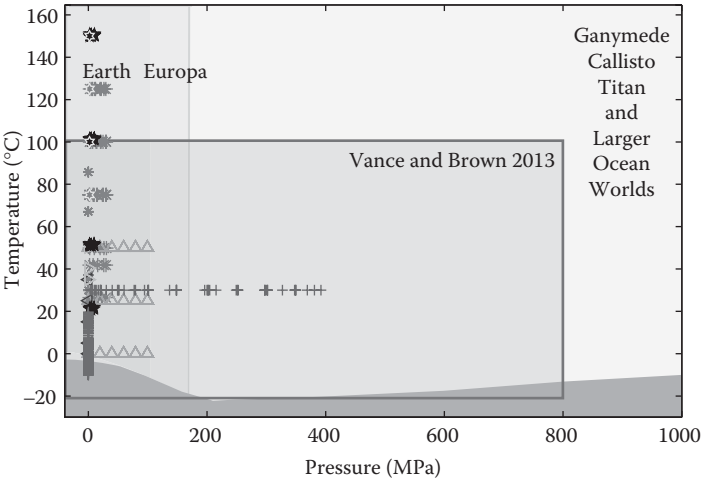

FIGURE 3.8
Pressures and temperatures of density measurements in the $MgSO_4$(aq) system illustrate that studies typically explore convenient laboratory conditions and conditions relevant to Earth's oceans. (Modified from *Cosmochim. Acta*, 110, Vance, S., J.M. Brown, 176–189, Copyright 2013, with permission from Elsevier.)

3.3.3 Properties of Nonaqueous Systems

Nonaqueous liquids play important roles in the chemistry and transport of materials at cryogenic temperatures. The best example of these interactions can be found on Titan, a moon of Saturn with a thick atmosphere and liquid hydrocarbon lakes. Methane and ethane form the liquid phase and are involved in an active cycle similar to the hydrologic cycle on Earth—these hydrocarbons form clouds, precipitate onto the surface, and pool in lakes at the North and South poles [Brown et al., 2010].

Titan also contains a vast inventory of organic molecules generated by photochemistry in the atmosphere. These species form solid aerosol particles that fall onto the surface, forming dunes in the equatorial regions [Lorenz et al., 2006]. Interactions of liquid hydrocarbons with solid phases include pluvial (via rainfall) and fluvial (via river) transport of particulates into the lakes [Lorenz et al., 2008], and may also generate landforms similar to limestone or gypsum karst structures on Earth [Malaska and Hodyss, 2014; Cornet et al., 2015].

In fact, the conditions present on Titan may be much more ubiquitous throughout the universe than those on Earth. The most common type of stable star in the universe is the M-dwarf (red dwarf), which is smaller and less luminous than the Sun (a G-dwarf). Planets in a safe orbit around such a star (1 AU) would receive a similar amount of radiation as Titan does—just enough to maintain liquid methane and ethane on the planet's surface. Since M-dwarfs are 10–100 times more abundant than G-dwarfs, it may be the case that Titan-like worlds are much more common than Earth-like worlds [Lunine, 2009]. Studies of the physical properties of nonaqueous liquids such as methane and ethane, therefore, may have implications for the exploration of many worlds.

The viscosities and densities of liquid methane, ethane, and propane have been reported at cryogenic temperatures [Haynes, 1973; Diller and Saber, 1981; Goodwin et al., 1973; Diller, 1982; Goodwin, 1977], as these are relevant for the liquefied natural gas industry. Thermal conductivities for these liquid hydrocarbons have also been measured [Younglove and Ely, 1987]. Values relevant to Titan surface conditions are shown in Table 3.1.

A recent study reported the complex dielectric constants of liquid methane and ethane at 90 K [Mitchell et al., 2015]. These loss tangents suggest that the northern lake Ligeia Mare of Titan is almost entirely comprised of methane, while the southern lake Ontario Lacus is more ethane-rich [Brown et al., 2008]. The loss tangent for methane ($2.86 \pm 1.01 \times 10^{-5}$) from Mitchell et al. is considerably lower compared with a previous study (1.14×10^{-3})

TABLE 3.1

Physical Properties of Liquid Hydrocarbons at Titan Surface Temperature (95 K)

Hydrocarbon	Viscosity (Pa·s)	Density (g/cm^3)	Thermal Conductivity (W/m·K)	Reference(s)
Methane	1.784×10^{-4}	0.4458	0.2155	Haynes [1973] and Hanley et al. [1977]
Ethane	1.073×10^{-3}	0.6468	0.261	Diller and Saber [1981], Goodwin et al. [1973], and Younglove and Ely [1987]
Propane	5.211×10^{-3}	0.7234	0.226	Diller [1982], Goodwin [1977], and Younglove and Ely [1987]

[Paillou et al., 2008], although the authors note that the Paillou et al. sample contained ~5% heavier hydrocarbons and is probably higher due to this contamination. Work with liquid alkane mixtures [Sen et al., 1992] indicates that the dielectric constant varies linearly with volume fraction as predicted by the Clausius–Mossotti equation [Hill et al., 1969]:

$$(\varepsilon'_{\mathrm{m}} - 1) / (\varepsilon'_{\mathrm{m}} + 2) = \Sigma_i 4\pi \upsilon_i \rho_i N_{\mathrm{A}} \alpha_i \; / \; 3M_i$$

where $\varepsilon'_{\mathrm{m}}$ is the dielectric constant of the mixture, and for the *i*th component of the mixture, υ_i is the volume fraction, ρ_i is the mass density, α_i is the electric polarizability, and M_i is the molecular weight.

Interactions of liquid hydrocarbons with solid organics at cryogenic temperatures have also been explored. Simulated Titan aerosols, termed "tholins," have been generated using various energy sources (cold plasma discharge, UV irradiation, etc.) and exposed to liquid hydrocarbons. These complex organics are relatively insoluble in liquid hydrocarbons, although adsorption onto the surface of these particles may enable chemistry at a gas–liquid interface as they fall through the atmosphere of Titan (for a review of Titan tholin formation and reactivity, see Cable et al., 2012).

Although tholins are not very soluble in liquid hydrocarbons, other organic species such as acetylene and HCN are believed to comprise approximately 1% and 2% of the Titan lakes, respectively [Cordier et al., 2009]. Acetylene is capable of polymerization on Titan [Raulin, 1987] and can serve as an energy source for methanogenic bacteria [McKay and Smith, 2005].

Less soluble species also have implications for Titan surface physical properties. Liquid ethane readily forms a co-crystal with solid benzene at 90 K, similar to a hydrated mineral on Earth [Cable et al., 2014; Vu et al., 2014]. These co-crystals may be present in evaporitic deposits around Titan lakes, and can affect evaporite properties such as particle size and dissolution rate. The crystal structure of the benzene–ethane co-crystal has recently been obtained at 90 K using synchrotron powder diffraction [Maynard-Casely et al., 2016].

Understanding the interaction of nonaqueous liquids with spacecraft materials is significant, both for interpreting data from the Huygens lander [Niemann et al., 2005; Lebreton et al., 2005] and for designing future *in situ* Titan missions. Methane behaves like a viscous non-Newtonian fluid just below its melting point (90.6 K), and adheres to materials such as aluminum, stainless steel, and PTFE with similar affinity [Kirichek et al., 2012]. Exposure of hydrocarbons to materials such as aluminum, steel, and titanium at cryogenic temperatures has been extensively explored in the liquefied natural gas industry, and no chemical reactivity has been reported [Kaufman, 1975].

Lorenz [2015] studied the effects of heat rejection for a Titan lake lander or submersible. For a lander with heat leaks on the order of 100 W/m^2 into the hydrocarbon liquid, experimental simulations indicate the formation of nitrogen bubbles (exsolvation) that may interfere with scientific measurements. Such heat leaks should be avoided by using thick insulation and rejecting as much heat as possible into the atmosphere.

3.3.3 Phase Transitions

Solid–liquid phase boundaries define multiple curves that are difficult to treat by extrapolation. Details of the melting point as a function of composition and temperature determine where liquids are stable in natural settings on Earth and other planets (e.g., Figures 3.9 and 3.10). Careful measurements of phase boundaries and crystallization kinetics in aqueous systems are enabled by high-resolution Raman spectroscopy [e.g., Bollengier et al., 2013; Cable et al., 2014].

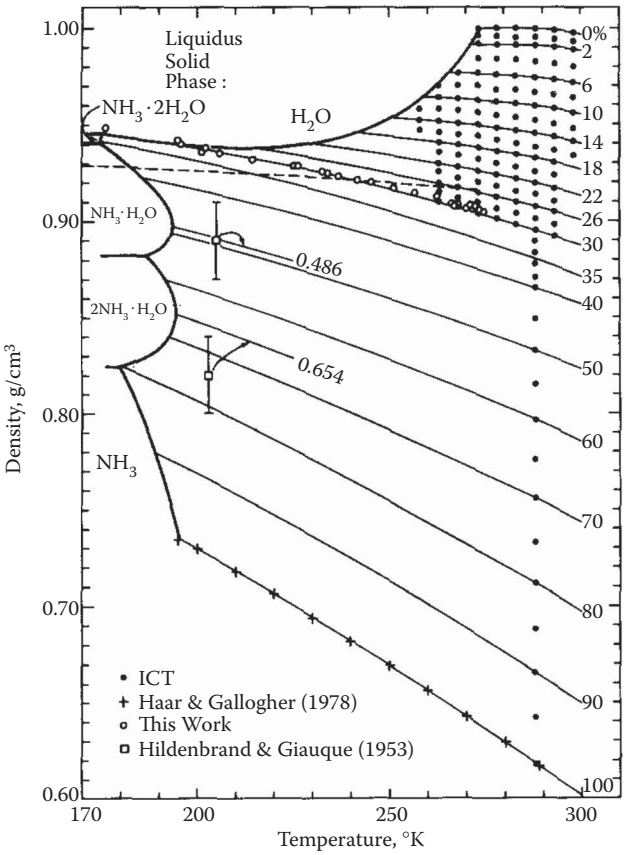

FIGURE 3.9
Phase diagram for ammonia at atmospheric pressure, showing a eutectic temperature of 170 K at 29 wt% and peritectic transitions separating different hydration states of ice at ~55 wt%, 185 K and 80 wt%, 180 K. (Reprinted from *Icarus*, 73(2), Croft, S.K., J.I. Lunine, J. Kargel, Equation of state of ammonia water liquid: Derivation and planetological applications, 279–293, Copyright 1988, with permission from Elsevier.)

3.4 Material Properties of Piezoelectric Materials at Cryogenic Temperatures

Piezoelectric materials are used for investigation of material thermodynamic properties, as described in the preceding text. They are also used as actuators in analytical instruments at cryogenic temperatures to investigate quantum physical phenomena at the nanometer scale, providing precision-controlled displacements for specimen stages used with scanning probes [Eriksson, 1996]. Piezoelectric materials are also used to actively tune superconducting radio frequency (SRF) cavities, enabling maintained resonance at high electromagnetic field intensity. Electro-motive and magneto-motive materials are also used at cryogenic temperatures as the active material in MEMS and NEMS sensor devices to investigate quantum and low temperature physical phenomena at the nanometer scale, for example [Collin et al., 2011]

The electro-mechanical properties of piezoelectric ceramics result from complex interdependency of both mechanical and electrical material properties, and are highly

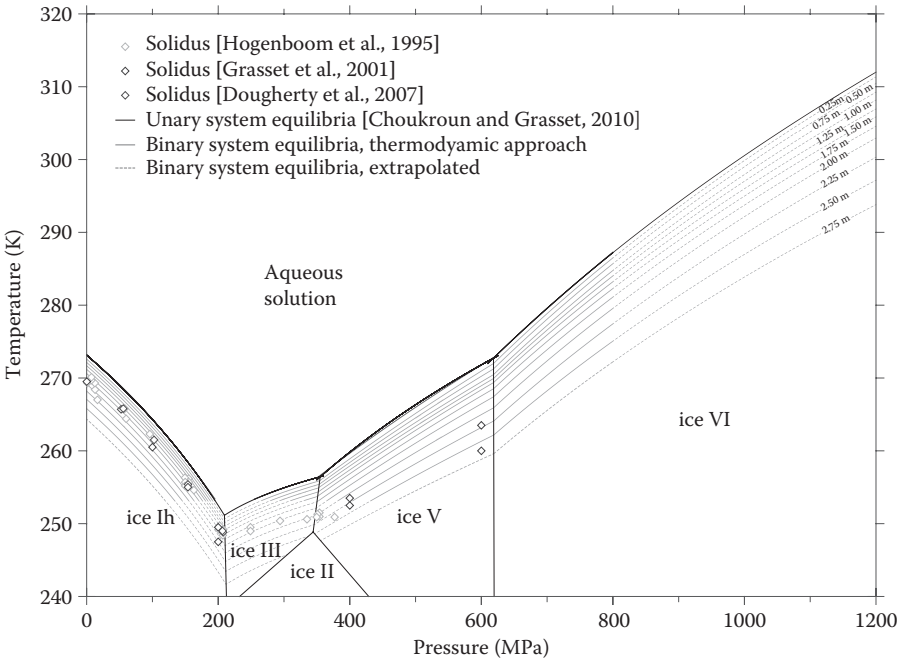

FIGURE 3.10
Suppression of the melting temperature of ices for increasing concentrations of $MgSO_4$ (aq), computed from available solidus data and Gibbs free energies for the fluid phase constructed from b-spline-based thermodynamic equations of state. (Courtesy of Olivier Bollengier, University of Washington, Seattle, Washington.)

temperature dependent. Advancing cryogenic instruments and sensors relying on piezoelectric elements requires characterizing their electromechanical coupling at low temperatures.

Lead zirconate tinate (PZT) is one of the most common piezoelectric materials utilized after quartz. Varying the percentages of constituent materials in PZT affects the crystallographic composition of the piezoelectric crystal. In pure bulk PZT crystals, compositions near the morphotropic boundary (between tetragonal and rhombohedral crystallographic phases) show the largest temperature dependence of pertinent electrical and mechanical material properties (dielectric constant and dissipation factor, respectively) [Zhuang et al., 1989]. Temperature–function relationships for PZT films have since been phenomenologically derived for several compositionally and crystallographically differing PZT films of varying thickness [Wolf and Trolier-McKinstry, 2004]. The variability in electro-mechanical coupling factors in differing composition of PZT films correlates with the differing values of Curie temperature. Furthermore, the relative electrical permittivity decreases with temperature. Decreasing permittivity diminishes the requisite electric field necessary to align poled domains (and thus create strain). Finally, the thermal expansion mismatch between the PZT film and substrate creates both strain and residual stress during and after temperature cycling [Wolf and Trolier-McKinstry, 2004], which further degrades the film's performance through low temperature cycling.

Piezoelectric stack actuator performance at low temperatures has been characterized in the development of active tuning of SRF cavities. In these studies, commercially available actuators are tested both electrically (dielectric loss) and mechanically (displacements) at cryogenic temperatures. In conjunction, thermal properties were also measured,

specifically heating due to dielectric loss. In general, Fouaidy's results coincide with the prior measurements and phenomenological derivations [Wolf and Trolier-McKinstry, 2004; Zhuang et al., 1989], showing a marked decrease in electro-mechanical conversion at low temperatures. The capacitance of the actuators decreases with temperature and mechanical performance. However, hysteresis in the mechanical response to applied voltages decreases to a negligible value at temperatures below 4 K. Despite approximately a 95% reduction in mechanical performance between the range of 300 K and 1.8 K, displacements on the order of several micrometers have been observed at the lowest temperatures. As temperatures decrease and mechanical performance diminishes, dielectric heating of the actuator diminishes. Despite significant degradation near 1.8 K, the commercial actuators perform in the range viable for deployment as active tuning devices for SRF cavities, with the benefits of reduced thermal contributions from dielectric heating and increased accuracy due to minimal response hysteresis [Fouaidy et al., 2005].

Neutron flux (~2.1×10^{15} N/cm^2) has been used to verify the efficacy of piezoelectric stack actuators for use in SRF cavities. These studies indicated negligible degradation due to radiation, and are thus viable in the radiation environment [Martinet, 2006]. Over the anticipated lifetime of an SRF cavity (>>3 Giga cycles), the effects of dynamic preloading on the electrical properties of the actuator stacks is predominantly linear throughout the range of temperatures (~2–300 K) [Fouaidy et al., 2007]. Increased preloading force corresponds to increased capacitance, and thereby mechanical performance. However, the proportionality of this linear correlation, or sensitivity, decreases with lower temperatures, with a 1000 N increase in preloading force corresponding to an increase in capacitance of 426 nF for actuators at 300 K, but only an increase of 16 nF for actuators at 2 K. Unlike the hysteresis in mechanical response to applied voltage at low temperatures, the change in electrical properties (capacitance) shows significant hysteresis during loading and unloading the piezoelectric actuators at $T = 2$ K [Fouaidy et al., 2007].

Piezoelectric material properties affecting electro-mechanical performance have been studied at cryogenic temperatures under various external conditions. In general, there is good agreement that the maximum mechanical displacement from a given voltage decreases with temperature. The degree of performance degradation is largely affected by the composition and associated crystallographic morphology of the piezoelectric device. Both bulk and thin-film exhibit reduced mechanical performance at a lower temperature, with more interfering phenomena in thin-film devices (thermal expansion mismatch, etc.). Despite the decrease in performance, piezoelectric material properties provide consistent mechanical response at cryogenic temperatures, with the added benefits of reduced dielectric heating and hysteresis. For applications in sensitive instrumentation and small-scale sensors, the loss in maximum displacement capabilities has little effect on the viability of the piezoelectric material.

3.5 Summary/Conclusions

The frontiers of physics and coupled human–robotic exploration beyond Earth drive progress in understanding the properties of low temperature materials. Planetary low-temperature materials comprise a large space of volatile compositions, involving complex rheologies, and multiple crystalline, amorphous, and liquid phases. Low temperature technologies enable innovative measurement techniques for probing fundamental properties such as sound speeds and phase boundaries, while fast computers enable detailed thermodynamic frameworks that will be necessary for future planetary exploration.

3.6 Acknowledgments

Some of the research reported in this chapter was conducted at the Jet Propulsion Laboratory (JPL), California Institute of Technology (Caltech), under a contract with the National Aeronautics and Space Administration (NASA). T.L. would like to acknowledge continuing support of his work by the Austrian Science Fund FWF (recently through START award Y391 and bilateral project I1392) and the European Research Council (ERC Starting Grant SULIWA). The authors would like to thank Jeffrey D. Hein, Robert P. Hodyss, and Victoria (Maria) Iglesias, JPL/Caltech, Pasadena, CA, for reviewing this chapter and providing valuable technical comments and suggestions.

References

Algara-Siller, G., O. Lehtinen, F.C. Wang, R.R. Nair, U. Kaiser, H.A. Wu, A.K. Geim, I.V. Grigorieva. Square ice in graphene nanocapillaries, *Nature*, 519 (2015), pp. 443–445.

Angell, C.A. Supercooled water, *Annu. Rev. Phys. Chem.*, 34 (1983), pp. 593–630.

Amann-Winkel, K., C. Gainaru, P.H. Handle, M. Seidl, H. Nelson, R. Bohmer, T. Loerting. Water's second glass transition, *Proc. Natl. Acad. Sci*. U. S. A., 110 (2013), p. 17720.

Andersson O., A. Inaba. Dielectric properties of high-density amorphous ice under pressure, *Phys. Rev. B.*, 74 (2006), p. 184201.

Andersson O. Glass–liquid transition of water at high pressure, *Proc. Natl. Acad. Sci.* U. S. A., 108 (2011), p. 11013.

Arakawa, M., N. Maeno. Effective viscosity of partially melted ice in the ammonia-water system, *Geophysi. Res. Lett.*, 21(14) (1994), pp. 1515–1518.

Arnold G.P., E.D. Finch, S.W. Rabideau, R.G. Wenzel. Neutron-diffraction study of ice polymorphs. III. Ice Ic, *J. Chem. Phys*. 49 (1968), p. 4365.

Baragiola R.A., in: V. Buch, J.P. Devlin (Eds.), *Water in Confining Geometries*, Heidelberg: Springer-Verlag (2003).

Benoit M., M. Bernasconi, P. Focher, M. Parrinello. New high-pressure phase of ice, *Phys. Rev. Lett.*, 76(16) (1996), pp. 2934–2936, doi:10.1103/PhysRevLett.76.2934.

Bernal J.D., R.H. Fowler. A theory of water and ionic solution, with particular reference to hydrogen and hydroxyl ions, *J. Chem. Phys.*, 1 (1933), p. 515.

Besson J.M., M. Kobayashi, T. Nakai, S. Endo, P. Pruzan. Pressure dependence of Raman linewidths in ices VII and VIII, *Phys. Rev. B.*, 55 (1997), p. 11191.

Besson J.M., P. Pruzan, S. Klotz, G. Hamel, B. Silvi, R.J. Nelmes, J.S. Loveday, R.M. Wilson, S. Hull. Variation of interatomic distances in Ice VIII to 10 GPa, *Phys. Rev. B.*, 49 (1994), p. 12540.

Bollengier, O., M. Choukroun, O. Grasset, E. Le Menn, G. Bellino, Y. Morizet, L. Bezacier, A. Oancea, C. Taffin, G. Tobie. Phase equilibria in the H_2O–CO_2 system between 250–330K and 0–1.7 GPa: Stability of the CO_2 hydrates and H_2O-ice VI at CO_2 saturation, *Geochim. Cosmochim. Acta.*, 119 (2013), pp. 322–339.

Bossa J.-B., K. Isokoski, M.S.d. Valois, H. Linnartz. Thermal collapse of porous interstellar ice, *Astron. Astrophys.*, 545 (2012), p. A82.

Bowron D.T., J.L. Finney, A. Hallbrucker, I. Kohl, T. Loerting, E. Mayer, A.K. Soper. The local and intermediate range structures of the five amorphous ices at 80 K and ambient pressure: A Faber-Ziman and Bhatia-Thornton analysis, *J. Chem. Phys.*, 125 (2006), p. 194502.

Brown, R. H., L.A. Soderblom, J.M. Soderblom, R.N. Clark, R. Jaumann, J.W. Barnes, C. Sotin, B. Buratti, K.H. Baines, P.D. Nicholson. The identification of liquid ethane in Titan's Ontario Lacus, *Nature*, 454 (2008), pp. 607–610.

Brown, R., J.P. Lebreton, H.J. Waite, (Eds.) *Titan from Cassini-Huygens*. Netherlands: Springer (2010).

Bruggeller, P., E. Mayer. Complete vitrification in pure liquid water and dilute aqueous solutions, *Nature*, 288 (1980), p. 569.

Burton E.F., W.F. Oliver. X-ray diffraction patterns of ice, *Nature*, 135 (1935), p. 505.

Cable, M.L., T.H Vu, R. Hodyss, M. Choukroun, M. J. Malaska, P. Beauchamp. Experimental determination of the kinetics of formation of the benzene-ethane co-crystal and implications for Titan, *Geophys. Res. Lett.*, 41(15) (2014), pp. 5396–5401.

Cable, M.L., S.M. Horst, R. Hodyss, P.M. Beauchamp, M.A. Smith, P.A. Willis. Low-temperature microchip nonaqueous capillary electrophoresis of aliphatic primary amines: Applications to Titan chemistry, *Chem. Rev.*, 112 (2012), pp. 1882–1909.

Carey, E., K. Mitchell, M. Choukroun, F. Zhong. Laboratory studies on the rheology of cryogenic slurries with implications for icy satellites, *Bull. Amer. Phys. Soc.*, 60(4) (2015), p. R2.00006.

Cartwright J.H.E., B. Escribano, C.I. Sainz-Diaz. The mesoscale morphologies of ice films: Porous and biomorphic forms of ice under astrophysical conditions, *Astrophys. J.*, 687 (2008), p. 1406.

Chen, C.T., F.J. Millero. Speed of sound in seawater at high-pressures, *J. Acoust. Soc. Am.*, 62(5) (1977), pp. 1129–1135.

Chen, C.T., L.S. Chen, F.J. Millero. Speed of sound in NaCl, $MgCl_2$, Na_2SO_4, and $MgSO_4$ aqueous-solutions as functions of concentration, temperature, and pressure, *J. Acous. Soc. Am.*, 63(6) (1978), pp. 1795–1800.

Choukroun, M., O. Grasset. Thermodynamic model for water and high-pressure ices up to 2.2 GPa and down to the metastable domain, *J. Chem. Phys.*, 127(12) (2007), p. 124506.

Choukroun, M., O. Grasset, G. Tobie, C. Sotin. Stability of methane clathrate hydrates under pressure: Influence on outgassing processes of methane on Titan, *Icarus*, 205(2) (2010), pp. 581–593.

Collin E., T. Moutonet, J.S. Heron, O. Bourgeois, Y.M. Bunkov, H. Godfrin. A tunable hybrid electromagnetomotive NEMS device for low temperature physics, *J. Low Temp Phys.*, 162(2011), p. 653.

Cooper, J., P. Cooper, E. Sittler, S. Sturner, A. Rymer. Old faithful model for radiolytic gas-driven cryovolcanism at Enceladus, *Planet. Space Sci.*, 57(13) (2009), pp. 1607–1620.

Conde, M.M., C. Vega, G.A. Tribello, B. Slater. The phase diagram of water at negative pressures: Virtual ices, *J. Chem. Phys*., 131 (2009), pp. 034510-1–034510-8.

Cordier, D., O. Mousis, J.I. Lunine, P. Lavvas, V. Vuitton. An estimate of the chemical composition of Titan's lakes, *Astrophys. J. Lett*., 707(2) (2009), pp. L128–L131.

Cornet, T., D. Cordier, T. Le Bahers, O. Bourgeois, C. Fleurant, S. Le Mouelic, N. Altobelli. Dissolution on Titan and on Earth: Towards the age of Titan's karstic landscapes, *J. Geophys. Res.*, (2015), doi10.1002/2014JE004738.

Diller, D.E., J.M. Saber. Measurements of the viscosity of compressed gaseous and liquid ethane, *Phys. A: Stat. Mech. Appl.*, 108(1) (1981), pp. 143–152.

Diller, D.E. Measurements of the viscosity of saturated and compressed liquid propane, *J. Chem. Eng. Data*, 27(3) (1982), pp. 240–243.

Croft, S.K., J.I. Lunine, J. Kargel. Equation of state of ammonia water liquid: Derivation and planetological applications, *Icarus*, 73(2) (1988), pp. 279–293.

Datchi, F., P. Loubeyre, R. Letoullec. Extended and accurate determination of the melting curves of argon, helium, ice (H_2O), and hydrogen (H_2), *Phys. Rev. B.*, 61(10) (2000), pp. 6535–6546.

Debenedetti P. G. Supercooled and glassy water, *J. Phys.: Condens. Matter*, 15 (2003), p. R1669.

Desch, S., J. Cook, T. Doggett, S. Porter. Thermal evolution of Kuiper belt objects, with implications for cryovolcanism, *Icarus*, (2009) doi:10.1016/j.icarus.2009.03.009.

De Yoreo, J.J., P.G Vekilov. Principles of crystal nucleation and growth, *Rev. Mineral. Geochem.*, 54 (2003), pp. 57–93.

Durham, W., S. Kirby, L. Stern. Flow of ices in the ammonia-water system, *J. Geophys. Res.: Solid Earth*, 98(B10), (1993), pp. 17667–17682.

Durham, W. B., S.H. Kirby, L.A. Stern. Steady-state flow of solid CO_2: Preliminary results, *Geophys. Res. Lett*., 26(23) (1999), pp. 493–3496.

Durham, W., S. Kirby, L. Stern. Rheology of water ice—Applications to satellites of the outer planets, *Ann. Rev. Earth Planet. Sci.*, 29 (2001), pp. 295–330.

Ehrenfreund, P., H.J. Fraser, J. Blum, J.H.E. Cartwright, J.M. Garcia-Ruiz, E. Hadamcik, A.C. Levasseur-Regourd, S. Price, F. Prodi, A. Sarkissian. Physics and chemistry of icy particles in the universe: Answers from microgravity, *Planet. Space Sci.*, 51 (2003), p. 473.

Elsaesser, M.S., K. Winkel, E. Mayer, T. Loerting. Reversibility and isotope effect of the calorimetric glass → Liquid transition of low-density amorphous ice, *Phys. Chem. Chem. Phys.*, 12(3) (2010), pp. 708–712.

Eluszkiewicz, J., D. Stevenson. Rheology of solid methane and nitrogen—Applications of Triton, *Geophys. Res. Lett.*, (ISSN 0094-8276) (1990), p. 17.

Eucken, A. The change in heat conductivity of solid metalloids with temperature, *Ann. Phys.*, 34 (1911), pp. 185–222.

Fagents, S.A. Considerations for effusive cryovolcanism on Europa: The post-Galileo perspective, *J. Geophys, Res. Planets*, 108(E12) (2003), p. 5139.

Faizullin, M.Z., A.V. Vinogradov, V.N. Skokov, V.P. Koverda. Fomation of gas hydrate during crystallization of ethane-saturated amorphous ice, *Russ. J. Phys. Chem.*, 88 (2014), p. 1706.

Falenty, A., T.C. Hansen, W.F. Kuhs, Formation and properties of Ice XVI obtained by emptying a type sII clathrate hydrate, *Nature*, 516 (2014), p. 231.

Fan X., D. Bing, J. Zhang, Z. Shen, J.-L. Kuo. Predicting the hydrogen bond ordered structures of Ice I_h, II, III, VI and Ice VII: DFT methods with localized based set, *Comp. Mater. Sci.*, 49 (2010), p. S170.

Finney, J., A. Hallbrucker, I. Kohl, A. Soper, D. Bowron. The local and intermediate range structures of the five amorphous ices at 80 K and ambient pressure: A Faber-Ziman and Bhatia-Thornton analysis. *Phys. Rev. Lett.*, 88(22) (2002), p. 225503.

Fortes, A., P. Grindrod, S. Trickett, L. Vocadlo. Ammonium sulfate on Titan: Possible origin and role in cryovolcanism, *Icarus*, 188(2007), pp. 139–153.

Fortes, A.D., I.G. Wood, J.P. Brodholt, L. Vocadlo. Ab initio simulation of the Ice II structure, *J. Chem. Phys.*, 119 (2003), p. 4567.

Fortes A.D., I.G. Wood, M. Alfredsson, L. Vocadlo, K.S. Knight. The incompressibility and thermal expansivity of D_2O Ice II determined by powder neutron diffraction, *J. Appl. Cryst.*, 38 (2005), p. 612.

Fouaidy, M., G. Martinet, N. Hammoudi, F. Chatelet, S. Blivet, A. Olivier, H. Saugnac. Proceedings from Particle Accelerator Conference (2005), p. 728.

Fouaidy, M., M. Saki, N. Hammoudi, L. Simonet. Electromechanical characterization of piezoelectric actuators subjected to a variable preloading force at cryogenic temperature. pp. 1–15, Report No. CARE-Note-2006-007-SRF, HAL Id: in2p3-00148455, https://hal.archives-ouvertes.fr/in2p3-00148455/document.

Frank, M., R.E. Aarestad, H.P Scott, V.B. Prakapenka. A comparison of ice VII formed in the H_2O, NaCl-H_2O, and CH_3OH-H_2O systems: Implications for H_2O-rich planets, *Phys. Earth Planet. Interiors*, 215(C) (2013), pp. 12–20. doi:10.1016/j.pepi.2012.10.010.

Frank M., C. Runge, H. Scott, S. Maglio, J. Olson, V. Prakapenka, G. Shen. Experimental study of the NaCl–H2O system up to 28 GPa: Implications for ice-rich planetary bodies, *Phys. Earth Planet. Interiors*, 155(12) (2006), pp. 152–162. doi:10.1016/j.pepi.2005.12.001.

Fuentes-Landete, V., C. Mitterdorfer, P.H. Handle, G.N. Ruiz, J. Bernard, A. Bogdan, M. Seidl, K. Amann-Winkel, J. Stern, S. Fuhrmann, T. Loerting. Crystalline and amorphous ices. In: P. G. Debenedetti, M. A. Ricci, and F. Bruni (Eds.), *Proceedings of the International School of Physics "Enrico Fermi," Volume 187: Water: Fundamentals as the Basis for Understanding the Environment and Promoting Technology.* Amsterdam: IOS and Bologna: SIF (2015), pp. 173–208.

Fukazawa, H., S. Ikeda, M. Oguro, T. Fukumura, S. Mae. Deuteron ordering in KOD-doped ice observed by neutron diffraction, *J. Phys. Chem. B.*, 106 (2002), pp. 6021.

Fukazawa, H., S. Ikeda, S. Mae. Incoherent inelastic neutron scattering measurements on ice XI; the proton-ordered phase of ice I_h doped with KOH, *Chem. Phys. Lett.*, 282 (1998), p. 215.

Gaidos, E.J. Cryovolcanism and the recent flow of liquid water on Mars, *Icarus*, 153(1) (2001), pp. 218–223.

Geiger P., C. Dellago, M. Macher, C. Franchini, G. Kresse, J. Bernard, J.S. Stern, T. Loerting. Proton ordering of cubic ice I_c: Spectroscopy and computer simulations, *J. Phys. Chem. C.*, 118(20) (2014), pp. 10989–10997.

Goodwin, R.D. Provisional thermodynamic functions of propane, from 85 to 700 K at pressures to 700 bar, *Nat. Bur. Stand*. (U.S.) Interagency Report NBSIR 77–860 (1977).

Goodwin, R.D., H.M. Roder, G.C Straty. Thermophysical properties of ethane, from 90 to 600 K at pressures to 700 bar, *Nat. Bur. Stand*. (U.S.), Technical Note 684 (1973).

Grasset, O., J. Schneider, C. Sotin. A study of the accuracy of mass-radius relationships for silicate-rich and ice-rich planets up to 100 Earth masses, *Astrophys. J.*, 693(1) (2009), p. 722.

Gross G.W., P.M. Wong, K. Humes. Concentration dependent solute redistribution at the ice–water phase boundary. III. Spontaneous convection. Chloride solutions, *J. Chem. Phys.*, doi:10.1063/1.434704, 67, (1977), pp. 5264–5274.

Gross G., A. Gutjahr, K. Caylor. Recent experimental work on solute redistribution at the ice/water interface. Implications for electrical properties and interface processes, *J. Phys.*, 48 (C1), (1987), pp. C1-527–C1-533. https://hal.archives-ouvertes.fr/jpa-00226318/document

Gross G.W., R. K. Svec. Effect of ammonium on anion uptake and dielectric relaxation in laboratory-grown ice columns, *J. Phys. Chem. B.*, 101(32) (1997): 6282–6284. doi:10.1021/jp963213c.

Grundy, W.M., B. Schmitt, E. Quirico. The temperature-dependent spectra of α and β nitrogen ice with application to Triton, *Icarus*, 105(1) (1993), pp. 254–258.

Guinier A., G.B. Bokii, K. Boll-Dornberger, J.M. Cowley, S. Durovic, H. Jagodzinski, P. Krishna, P.M. De Wolff, B.B. Zvyagin, et al. Nomenclature of polytype structures. Report of the International Union of Crystallography Ad hoc Committee on the Nomenclature of Disordered, Modulated and Polytype Structures, *Acta Crystallogr.*, A40 (1984), p. 399.

Hallbrucker, A., E. Mayer, G. Johari. Glass-liquid transition and the enthalpy of devitrification of annealed vapor-deposited amorphous solid water: A comparison with hyperquenched glassy water, *J. Phys. Chem.*, 93(12)(1989), pp. 4986–4990.

Handa Y.P., O. Mishima, E. Whalley. High-density amorphous ice. III. Thermal properties, *J. Chem. Phys.*, 84 (1986), p. 2766.

Hanley, H.J.M., W.M. Haynes, R.D. McCarty. The viscosity and thermal conductivity coefficients for dense gaseous and liquid methane. *J. Phys. Chem. Ref. Data*, 6(597) (1977), pp. 597–609.

Hansen, T.C., A. Falenty, W.F. Kuhs. Modelling ice I_c of different origin and stacking-faulted hexagonal ice using neutron powder diffraction data, *Phys. Chem. Ice, Proc. Int. Conf.*, 11th (2007) 201.

Hassanali, A.A., J. Cuny, V. Verdolino, M. Parrinello. Aqueous solutions: State of the art in ab initio molecular dynamics, *Phil. Trans. Royal Soc. London A: Math., Phys. Eng. Sci.*, 372(2011) (2014), p. 20120482.

Haynes, W.M. Viscosity of saturated liquid methane, *Physica*, 70 (1973), pp. 410–412.

Hendricks, S.B., M.E. Jefferson. On the optical anisotropy of molecular crystals, *J. Opt. Soc. Am.*, 23 (1933), pp. 299–307.

Hermann, A., N.W. Ashcroft, R. Hoffmann. High pressure ices, *PNAS.*, 109(3) (2012), pp. 745–750. doi:10.1073/pnas.1118694109/-/DCSupplemental/Appendix.pdf.

Herrero, C.P., R. Ramírez,Topological characterization of crystalline ice structures from coordination sequences, *Phys. Chem. Chem. Phys.*, 15(2013), p. 16676.

Hill, N.E., W.E. Vaughan, A.H. Price, M. Davis. *Dielectric Properties and Molecular Behavior*. New York, NY: Van Nostrand (1969).

Hobbs P.V. *Ice Physics*. Oxford: Clarendon Press (1974).

Hogenboom, D.L., J.S. Kargel, J.P. Ganasan, L. Lee. Magnesium sulfate-water to 400 MPa using a novel piezometer: Densities, phase equilibria, and planetological implications, *Icarus*, 115(2) (1995), pp. 258–277.

Hogenboom, D.L., J.S. Kargel, G.J. Consolmagno, T.C. Holden, L. Lee, M. Buyyounouski. The ammonia-water system and the chemical differentiation of icy satellites, *Icarus*, 128(1) (1997), pp. 171–180.

Hussmann, H., F. Sohl, T. Spohn. Subsurface oceans and deep interiors of medium-sized outer planet satellites and large trans-neptunian objects, *Icarus*, 185 (2006), pp. 258–273.

Ioppolo, S., H.M. Cuppen, C. Romanzin, E.F.v. Dishoeck, H. Linnartz. Water formation at low temperatures by surface O_2 hydrogenation I: Characterization of ice penetration, *Phys. Chem. Chem. Phys.*, 12 (2010), p. 12065.

Johannessen, B., P. Kluth, D.J. Llewellyn, G.J. Foran, D.J. Cookson, M.C. Ridgway. Amorphisation of embedded Cu nanocrystals by ion irradiation, *Appl. Phys. Lett.*, 90(7) (2007), p. 073119.

Johari, G.P. Liquid state of low-density pressure-amorphized ice above its T_g, *J. Phys. Chem. B.*, 102 (1998), p. 4711.

Johari G. P., A. Hallbrucker, and E. Mayer. The glass–liquid transition of hyperquenched water, *Nature*, 330, pp. 552–553, doi:10.1038/330552a0.

Jorgensen, J.D., R.A. Beyerlein, N. Watanabe, T.G. Worlton. Structure of D_2O Ice VIII from in situ powder neutron diffraction, *J. Chem. Phys.*, 81 (1984), p. 3211.

Jorgensen, J.D., T.G. Worlton. Disordered structure of D2O ice VII from in situ neutron powder diffraction, *J. Chem. Phys.*, 83 (1985), p. 329.

Journaux B., I. Daniel, H. Cardon, S. Petitgirard, J. Perrillat, R. Caracas, and M. Mezouar. Experimental determination of salt partition coefficients between aqueous fluids, ice VI and ice VII: Implication for the composition of the deep ocean and the geodynamics of large icy moons and water rich planets, EGU2015-9503-3, EGU General Assembly 2015, Vienna, April 2015. http://meetingorganizer.copernicus.org/EGU2015/EGU2015-9503-3.pdf.

Kamb, B. Ice II: A proton-ordered form of ice, *Acta Crystallogr.*, 17 (1964), p. 1437.

Kamb, B., W.C. Hamilton, S.J. LaPlaca, A. Prakash. Ordered proton configuration in ice II, from single-crystal neutron diffraction, *J. Chem. Phys.*, 55 (1971), p. 1934.

Kargel, J. Cryovolcanism on the icy satellites, *Earth Moon Planets*, 67(1) (1994), pp. 101–113.

Kaufman, J. G. *Properties of Materials for Liquefied Natural Gas Tankage*. Baltimore, MD: American Society for Testing and Materials (1975).

Kirichek, O., A.J. Church, M.G. Thomas, D. Cowdery, S.D. Higgins, M.P. Dudman, Z.A. Bowden. *Cryogenics*, 52(7–9) (2012), pp. 325–330.

Klotz S., L. Bove, T. Strässle, T. Hansen, A. Saitta. The preparation and structure of salty ice VII under pressure, *Nat. Mater.*, 8 (2009), pp. 405–409.

Knight, C., S.J. Singer. Prediction of a phase transition to a hydrogen bond ordered form of ice VI, *J. Phys. Chem. B.*, 109 (2005), p. 21040.

Knight, C., S.J. Singer. A reexamination of the Ice III/IX hydrogen bond ordering phase transition, *J. Chem. Phys.*, 125 (2006), p. 064506/1.

Knight, C., S.J. Singer, J.-L. Kuo, T.K. Hirsch, L. Ojamae, M.L. Klein. Hydrogen bond topology and the Ice VII/VIII and I_h/XI proton ordering phase transitions, *Phys. Rev. E.*, 73 (2006), p. 056113/1.

Knight, C., S.J. Singer. Hydrogen bond ordering in ice V and the transition to ice XIII, *J. Chem. Phys.*, 129 (2008), 164513/1.

Kohl, I., E. Mayer, A. Hallbrucker. The glassy water–cubic ice system: A comparative study by x-ray diffraction and differential scanning calorimetry, *Phys. Chem. Chem. Phys.*, 2 (2000), p. 1579.

Kohl, I., L. Bachmann, A. Hallbrucker, E. Mayer, T. Loerting. Liquid-like relaxation in hyperquenched water at ≤140 K, *Phys. Chem. Chem. Phys.*, 7 (2005), p. 3210.

Köster, K.W., V. Fuentes Landete, A. Raidt, M. Seidl, C. Gainaru, T. Loerting, R. Böhmer. Dynamics enhanced by HCl doping triggers full Pauling entropy release at the ice XII-XIV transition. *Nat. Commun.*, 6 (2015), pp. 1–7.

Kuhs, W.F.E., J.L. Finney, C. Vettier, D.V. Bliss. Structure and hydrogen ordering in ices VI, VII, and VIII by neutron powder diffraction, *J. Chem. Phys.*, 81 (1984), p. 3612.

Kuhs, W.F., M.S. Lehmann. *Water Science Reviews 2*. In: F. Franks (Ed.), Cambridge: Cambridge University Press, (1986), p. 1.

Kuhs, W.F., D.V. Bliss, J.L. Finney. High-resolution neutron powder diffraction study of ice Ic, *J. Phys., Colloq.* (1987), p. C1.

Kuhs, W.F., C. Lobban, J.L. Finney. Partial H-ordering in high pressure ices III and V, *Rev. High Press. Sci. Technol.*, 7 (1998), p. 1141.

Kuhs, W.F. *Physics and Chemistry of Ice*. Royal Society of Chemistry (2007). http://books.google.com/books?id=sFp56qUc2HMC&pg=PA249&dq=intitle:Physics+and+Chemistry+of+Ice+Proceeding&hl=&cd=1&source=gbs_api

Kuo, J.-L., M.L. Klein, W.F. Kuhs. The effect of proton disorder on the structure of ice-I_h: A theoretical study, *J. Chem. Phys.*, 123 (2005), pp. 134505/1.

Kuo, J.-L., W.F. Kuhs. A first principles study on the structure of ice-VI: Static distortion, molecular geometry, and proton ordering, *J. Phys. Chem. B.*, 110 (2006), p. 3697.

LaPlaca, S.J., W.C. Hamilton, B. Kamb, A. Prakash. On a nearly proton-ordered structure for ice IX, *J. Chem. Phys.*, 58 (1973), p. 567.

Lebreton, J.-P., O. Witasse, C. Sollazzo, T. Blanquaert, P. Couzin, A.M. Schipper, J.B. Jones, D.L. Matson, L.I. Gurvits, D.H. Atkinson. An overview of the descent and landing of the Huygens probe on Titan, *Nature*, 438 (2005), pp. 758–764.

Leger, A., F. Selsis, C. Sotin, T. Guillot, D. Despois, D. Mawet, M. Ollivier, A. Labeque, C. Valette, F. Brachet. A new family of planets? "Ocean Planets". *Icarus*, 169(2) (2004), pp. 499–504.

Leliwa-Kopystynski, J., M. Maruyama, T. Nakajima. The water-ammonia phase diagram up to 300 MPa: Application to icy satellites, *Icarus*, 159 (2002), pp. 518–528.

Lemmon E.W., M.L. Huber, M.O. McLinden, NIST standard reference database 23: Reference fluid thermodynamic and transport properties-REFPROP, Version 9.1, National Institute of Standards and Technology, Standard Reference Data Program, Gaithersburg (2013).

Lin, C., Trusler. The speed of sound and derived thermodynamic properties of pure water at temperatures between (253 and 473) K and at pressures up to 400 MPa, *J. Chem. Phys.*, 136 (2012), p. 094511.

Lobban, C., J.L. Finney, W.F. Kuhs. The structure and ordering of ices III and V, *J. Chem. Phys.*, 112 (2000), p. 7169.

Loerting, T., K. Winkel, M. Seidl, M. Bauer, C. Mitterdorfer, P.H. Handle, C.G. Salzmann, E. Mayer, J.L. Finney, D.T. Bowron. How many amorphous ices are there?, *Phys. Chem. Chem. Phys.*, 13 (2011), p. 8783.

Loerting, T., V.V. Brazhkin, T. Morishita. Multiple amorphous-amorphous transitions, *Adv. Chem. Phys.*, 143 (2009), p. 29.

Lokotosh, T.V., N.P. Malomuzh. Proton ordering in cubic ice, *Khim. Fiz.*, 12 (1993), pp. 897–907.

Londono, J.D., W.F. Kuhs, J.L. Finney. Neutron diffraction studies of ices III and IX on under-pressure and recovered samples, *J. Chem. Phys.*, 98 (1993), p. 4878.

Lonsdale, K. Diamagnetic and paramagnetic anisotropy of crystals, *Rep. Prog. Phys.*, 4 (1937), p. 368.

Lorenz, R.D., S.E. Shandera. Physical properties of ammonia-rich ice: Application to Titan, *Geophys. Res. Lett.*, 28, 2 (2001), pp. 215–218.

Lorenz, R.D., S. Wall, J. Radebaugh, G. Boubin, E. Reffet, M. Janssen, E. Stofan, R. Lopes, R. Kirk, C. Elachi, C., et al. Titan's damp ground: Constraints on Titan surface thermal properties from the temperature evolution of the Huygens GCMS inlet, *Science*, 312, 5774 (2006), pp. 724–727.

Lorenz, R.D., R.M. Lopes, F. Paganelli, J.I. Lunine, R.L. Kirk, K.L. Mitchell, L.A. Soderblom, E.R. Stofan, G. Ori, M. Myers, M., et al. Fluvial channels on Titan: Initial Cassini RADAR observations, *Planet. Space Sci.*, 56, 8 (2008), pp. 1132–1144.

Lorenz, R.D. Heat rejection in the Titan surface environment: Potential impact on science investigations, *J. Thermophys. Heat Trans.*, 1–9 (2015), pp. 1.T4608.

Lunine, J.I. Saturn's Titan: Jonathan I. Lunine. A strict test for life's cosmic ubiquity, *Proc. Am. Phil. Soc*. 153(4) (2009), pp. 403–418.

Malaska, M.J., R. Hodyss. Dissolution of benzene, naphthalene, and biphenyl in a simulated Titan lake, *Icarus*, 242 (2014), pp. 74–81.

Martin-Conde, M., L.G. MacDowell, C. Vega. Computer simulation of two new solid phases of water: Ice XIII and ice XIV, *J. Chem. Phys.*, 125 (2006), p.116101.

Marion, G., J. Kargel, D. Catling, D., J. Lunine. Modeling ammonia–ammonium aqueous chemistries in the solar system's icy bodies, *Icarus*, 220 (2012), pp. 932–946.

Matsuo T., Y. Tajima, H. Suga. Calorimetric study of a phase transition in D_2O Ice I_h doped with KOD: Ice XI, *J. Phys. Chem. Solids.*, 47 (1986), pp. 165.

Mayer, E., A. Hallbrucker. Cubic ice from liquid water, *Nature*, 325 (1987) 601.

Mayer, E. New method for vitrifying water and other liquids by rapid cooling of their aerosols, *J. Appl. Phys.*, 58 (1985), p. 663.

Mayer, E., R. Pletzer. Astrophysical implications of amorphous Ice—A microporous solid, *Nature*, 319 (1986), p. 298.

Maynard-Casely H., R. Hodyss, M. Cable and T. Vu. A co-crystal between benzene and ethane, an evaporite material for Saturn's moon Titan, *IUCr J.*, (2016), accepted for publication.

McKay, C.P., H.D. Smith. Possibilities for methanogenic life in liquid methane on the surface of Titan, *Icarus*, 178, 1 (2005), pp. 274–276.

Mehling, H., F. Cabeza. *Heat and Cold Storage with PCM*, Springer Science & Business Media, (2008), p. 308.

Militzer, B., H.F. Wilson. New phases of water ice predicted at megabar pressures, *Phys. Rev. Lett.*, 105(19) (2010), p. 195701.

Millero, F.J., C.A. Chen. The speed of sound in mixtures of the major sea salts–a test of Young's rule for adiabatic PVT properties, *J. Solut. Chem.*, 14(4)(1985), pp. 301–310.

Minceva-Sukarova, B., W.F. Sherman, G.R. Wilkinson. A high pressure spectroscopic study on ice III-ice IX, disordered-ordered transition, *J. Mol. Struct.*, 115 (1984), p. 137.

Mishima, O., S. Endo. Melting curve of ice VII, *J. Chem. Phys.*, 68(10) (1978), pp. 4417–4418. doi:10.1063/1.435522.

Mishima, O., L.D. Calvert, E. Whalley. Melting ice I at 77 K and 10 kbar: A new method of making amorphous solids, *Nature*, 310 (1984), p. 393.

Mishima, O., L.D. Calvert, E. Whalley. An apparently first-order transition between two amorphous phases of ice induced by pressure, *Nature*, 314 (1985), p. 76.

Mishima, O. Melting of the precipitated ice IV in LiCl aqueous solution and polyamorphism of water, *J. Phys. Chem. B.*, 115(48) (2011), pp. 14064–14067.

Mitchell, K. L., M.B. Barmatz, C.S. Jamieson, R.D. Lorenz, J.I. Lunine. Laboratory measurements of cryogenic liquid alkane microwave absorptivity and implications for the composition of Ligeia Mare, Titan, *Geophys. Res. Lett.*, 42, 5 (2015), pp. 1340–1345.

Mitterdorfer, C., M. Bauer, T. Loerting.Clathrate hydrate formation after CO_2–H_2O vapour deposition, *Phys. Chem. Chem. Phys.*, 13 (2011), p. 19765.

Mitterdorfer, C., M. Bauer, T.G.A. Youngs, D.T. Bowron, C.R. Hill, H.J. Fraser, J.L. Finney, T. Loerting. Small-angle neutron scattering study of micropore collapse in amorphous solid water, *Phys. Chem. Chem. Phys.*, 16 (2014), p. 16013.

Murray, B.J., D.A. Knopf, A.K. Bertram. The formation of cubic ice under conditions relevant to earth's atmosphere, *Nature*, 434 (2005), p. 202.

Nelmes, R.J., J.S. Loveday, T. Straessle, C.L. Bull, M. Guthrie, G. Hamel, S. Klotz. Annealed high-density amorphous ice under pressure, *Nat. Phys.*, 2 (2006), p. 414.

Niemann, H.B., S.K. Atreya, S.J. Bauer, G.R. Carignan, J.E. Demick, R.L. Frost, D. Gautier, J.A. Haberman, D.M. Harpold, D.M. Hunten, et al. The abundance of constituents of Titan's atmosphere from the GCMS instrument on the Huygens probe, *Nature*, 438 (2005), pp. 779–784.

Nishibata, K., E. Whalley. Thermal effects of the transformation ice III–IX, *J. Chem. Phys.*, 60 (1974), p. 3189.

Noya, E.G., M.M. Conde, C. Vega. Computing the free energy of molecular solids by the Einstein molecule approach: Ices XIII and XIV and a simple model of proteins, *J. Chem. Phys.*, 129 (2008), p. 16.

Paillou, P., K. Mitchell, S. Wall, G. Ruffie, C. Wood, R. Lorenze, E. Stofan, J. Lunine, R. Lopes, P. Encrenaz. Microwave dielectric constant of liquid hydrocarbons: Application to the depth estimation of Titan's lakes, *Geophys Res. Lett.* 35 (2008) L05202.

Parkkinen, P., S. Riikonen, L. Halonen. Ice XI: Not that ferroelectric, *J. Phys. Chem. C.*, 118(2014), p. 26264.

Pauling, L. The structure and entropy of ice and of other crystals with some randomness of atomic arrangement, *J.Am. Chem. Soc.*, 57(12) (1935), pp. 2680–2684.

Petrenko, V.F., R.W. Whitworth. *Physics of Ice*. Oxford University Press, 2002.

Pistorius, C.W.F.T., M.C. Pistorius, J.P. Blakey, L.J. Admiraal. Melting curve of ice VII to 200 kbar. *J. Chem. Phys.*, 38(3) (1963), p. 600. doi:10.1063/1.1733711.

Pitzer, K. *Activity Coefficients in Electrolyte Solutions*. CRC Press, Boca Raton, FL, (1991).

Poole, P.H., F. Sciortino, U. Essmann, H.E. Stanley. Phase behaviour of metastable water, *Nature*, 360 (1992), pp. 324–328.

Pruzan, P., J.C. Chervin, B. Canny. Determination of the D_2O ice VII–VIII transition line by Raman scattering up to 51 GPa, *J. Chem. Phys.*, 97 (1992), pp. 718–721.

Pruzan, P., J.C. Chervin, E. Wolanin, B. Canny, M. Gauthier, M. Hanfland. Phase diagram of ice in the VII–VIII–X domain. Vibrational and structural data for strongly compressed ice VIII, *J. Raman Spectrosc.*, 34 (2003), p. 591.

Pruzan, P., J.C. Chervin, M. Gauthier. Raman spectroscopy investigation of ice VII and deuterated ice VII to 40 GPa. Disorder in ice VII, *Europhys. Lett.*, 13 (1990), p. 81.

Quirico, E., S. Douté, B. Schmitt, C. de Bergh, D.P. Cruikshank, T.C Owen, T.R Geballe, T.L Roush. Composition, physical state, and distribution of ices at the surface of Triton, *Icarus*, 139 (1999), pp. 159–178.

Raulin, F. Organic chemistry in the oceans of Titan, *Adv. Space Res.*, 7(5) (1987), pp. 71–81.

Röttger, K., A. Endriss, J. Ihringer, S. Doyle, W.F. Kuhs. Lattice constants and thermal expansion of H_2O and D_2O Ice I_h between 10 and 265 K, *Acta Crystallogr.*, B50 (1994), p. 644.

Salzmann, C.G., P.G. Radaelli, A. Hallbrucker, E. Mayer, J.L. Finney. The preparation and structures of hydrogen ordered phases of ice, *Science*, 311 (2006a), p. 1758.

Salzmann, C.G., A. Hallbrucker, J.L. Finney, E. Mayer. Raman spectroscopic study of hydrogen ordered ice XIII and of its reversible phase transition to disordered ice V, *Phys. Chem. Chem. Phys.*, 8 (2006b), p. 3088.

Salzmann, C.G., A. Hallbrucker, J.L. Finney, E. Mayer. Raman spectroscopic features of hydrogen-ordering in ice XI, *Chem. Phys. Lett.*, 429 (2006c), p. 469.

Salzmann, C.G., T. Loerting, S. Klotz, P.W. Mirwald, A. Hallbrucker, E. Mayer. Isobaric annealing of high-density amorphous ice between 0.3 and 1.9 GPa: In situ density values and structural changes, *Phys. Chem. Chem. Phys.*, 8 (2006d), p. 386.

Salzmann, C.G., P.G. Radaelli, E. Mayer, J.L. Finney. Ice XV: A new thermodynamically stable phase of ice, *Phys. Rev. Lett.*, 103 (2009), p. 105701/1.

Salzmann, C.G., P.G. Radaelli, J.L. Finney, E. Mayer. A calorimetric study on the low temperature dynamics of doped ice V and its reversible phase transition to hydrogen ordered ice XIII, *Phys. Chem. Chem. Phys.*, 10 (2008), p. 6313.

Sands, D.E. *Introduction to Crystallography*. Dover Publications (1975).

Sanloup, C., S.A. Bonev, M. Hochlaf, H.E. Maynard-Casely. Reactivity of xenon with ice at planetary conditions. *Phys. Rev. Lett.*, 110(26) (2013), p. 265501.

Schubert, G., J. Anderson, T. Spohn, W. McKinnon. Interior composition, structure and dynamics of the Galilean satellites. In: F. Bagenal, et al. (Eds.), *Jupiter: The Planet, Satellites and Magnetosphere* (2004), pp. 281–306.

Seidl M., M.S. Elsaesser, K. Winkel, G. Zifferer, E. Mayer, T. Loerting. Volumetric study consistent with a glass-to-liquid transition in amorphous ices under pressure, *Phys. Rev. B*, 83 (2011), p. 100201.

Sellberg, J.A. et al. Ultrafast x-ray probing of water structure below the homogeneous ice nucleation temperature, *Nature*, 510 (2014), p. 381.

Sen, A.D., V.G. Anicich, T. Arakelian. Dielectric constant of liquid alkanes and hydrocarbon mixtures, *J. Phys. D: Appl. Phys.*, 25 (1992), pp. 516–521.

Sepúlveda, A., E. Leon-Gutierrez, M. Gonzalez-Silveira, C. Rodríguez-Tinoco, M.T. Clavaguera-Mora, J. Rodríguez-Viejo. Glass transition in ultrathin films of amorphous solid water, *J. Chem. Phys.*, 137 (2012), p. 244506.

Sestak, J., J.J. Mares, P. Hubik. *Glassy, Amorphous, and Nano-Crystalline Materials, Thermal Physics, Analysis, Structure and Properties*. Springer, New York, (2011).

Singer, S.J., J.-L. Kuo, T.K. Hirsch, C. Knight, L. Ojamaee, M.L. Klein. Hydrogen-bond topology and the ice VII/VIII and ice I_h/XI proton-ordering phase transitions, *Phys. Rev. Lett.*, 94 (2005), p. 135701/1.

Somayazulu, M., J. Shu, C.-s. Zha, A.F. Goncharov, O. Tschauner, H.-k. Mao, R.J. Hemley. In situ high-pressure x-ray diffraction study of H_2O Ice VII, *J. Chem. Phys.*, 128 (2008), p. 064510/1.

Song, M., H. Yamawaki, H. Fujihisa, M. Sakashita, K. Aoki. Infrared investigation on ice VIII and the phase diagram of dense ices, *Phys. Rev. B.*, 68 (2003), p. 014106/1.

Sotin, C., O. Grasset, A. Mocquet. Mass-radius curve for extrasolar earth-like planets and ocean planets, *Icarus*, 191(1) (2007), pp. 337–351.

Speedy, R.J., C.A. Angell. Isothermal compressibility of supercooled water and evidence for a thermodynamic singularity at−45°C, *J. Chem. Phys.*, 65 (1976), pp. 851–858.

Stachurski, Z.H. On structure and properties of amorphous materials, *Materials*, 4 (2011), pp. 1564–1598.

Stanley, H.E., S.V. Buldyrev, M. Canpolat, O. Mishima, M.R. Sadr-Lahijany, A. Scala, F.W. Starr. The Puzzling Behavior of Water at Very Low Temperature, Proceedings—International Meeting on Metastable Fluids, *Phys. Chem. Chem. Phys.*, 2 (2000), p. 1551.

Stevenson, K.P., G.A. Kimmel, Z. Dohnalek, R.S. Smith, B.D. Kay. Controlling the morphology of amorphous solid water, *Science*, 283 (1999), p. 1505.

Tajima, Y., T. Matsuo, H. Suga. Calorimetric study of phase transition in hexagonal ice doped with alkali hydroxides, *J. Phys. Chem. Solids*, 45 (1984), p. 1135.

Tammann, G. Ueber die Grenzen des festen Zustandes IV, *Ann. Phys.*, (1900), p. 1.

Tobie, G., O. Grasset, J.I. Lunine, A. Mocquet, C. Sotin. Titan's internal structure inferred from a coupled thermal-orbital model. *Icarus*, 175(2) (2005), pp. 496–502.

Tribello, G.A., B. Slater, C.G. Salzmann. A blind structure prediction of ice XIV, *J. Am. Chem. Soc.*, 128 (2006), p. 12594.

Umemoto, K., R.M. Wentzcovitch. Two-stage dissociation in $MgSiO_3$ post-perovskite, *Earth Planet. Sci. Lett.*, 311(3) (2011), pp. 225–229.

Van Sciver, S.W. *Helium Cryogenics*, International Cryogenics Monograph Series, 17 Springer Science (2012), doi10.1007/978-1-4419-9979-5_2.

Vance, S., J.M. Brown. Layering and double-diffusion style convection in Europa's ocean, *Geochim. Cosmochim. Acta*, 110 (2013), pp. 176–189.

Vance, S., J. Goodman. *Oceanography of an Ice Covered Moon*. Europa: Arizona University Press (2009), pp. 459–482.

Vance, S., J. Harnmeijer, J. Kimura, H. Hussmann, B. deMartin, J.M. Brown. Hydrothermal systems in small ocean planets, *Astrobiology*, 7(6) (2007), pp. 987–1005.

Vance, S., M. Bouffard, M. Choukroun, C. Sotin. Ganymede's internal structure including thermodynamics of magnesium sulfate oceans in contact with ice, *Planet. Space Sci.*, 96 (2014), pp. 62–70.

Vu, T.H., M.L. Cable, M. Choukroun, R. Hodyss, P. Beauchamp. Formation of a new benzene-ethane co-crystalline structure under cryogenic conditions, *J. Phys. Chem. A*, 118(23) (2014), pp. 4087–4094.

Wang, Y., H. Liu, J. Lv, L. Zhu, H. Wang, Y. Ma. High pressure partially ionic phase of water ice, *Nat. Commun.*, 2 (2011), p. 563.

Weeks, W.F., S.F. Ackley. *The Geophysics of Sea Ice*. In: Norbert Untersteiner (Ed.), 9 164. NATO ASI Series. Springer US(1986).

Whalley, E., Cubic ice in nature, *J. Phys. Chem.*, 87 (1983), p. 4174.

Whalley, E., J.B.R. Heath, D.W. Davidson. Ice IX: An antiferroelectric phase related to ice III, *J. Chem. Phys.*, 48 (1968), p. 2362.

Whalley, E., D.W. Davidson, J.B.R. Heath. Dielectric properties of ice VII. Ice VIII: A new phase of ice, *J. Chem. Phys.*, 45 (1966), p. 3976.

Wilson, H.F., et al. Superionic to superionic phase change in water: Consequences for the interiors of Uranus and Neptune, *Phys. Rev. Lett.*, 110 (2013), p. 151102.

Winkel, K., M.S. Elsaesser, E. Mayer, T. Loerting. Water polyamorphism: Reversibility and (dis)continuity, *J. Chem. Phys.*, 128 (2008), p. 044510.

Winkel, K., E. Mayer, T. Loerting. Equilibrated high-density amorphous ice and its first-order transition to the low-density form, *J. Phys. Chem. B*, 115 (2011), p. 14141.

Wolf, R.A., S. Trolier-McKinstry. Temperature dependence of the piezoelectric response in lead zirconate titanate films, *J. Appl. Phys.*, 95(3) (2004).

Yamashita, Y., M. Kato, M. Arakawa. Experimental study on the rheological properties of polycrystalline solid nitrogen and methane: Implications for tectonic processes on Triton. *Icarus J.*, 207(2) (2010), pp. 972–977, doi:10.1016/j.icarus.2009.11.032.

Yoshimura, Y., S.T. Stewart, M. Somayazulu, H.-k. Mao, R.J. Hemley. High-pressure x-ray diffraction and Raman spectroscopy of ice VIII, *J. Chem. Phys.*, 124 (2006), p. 024502/1.

Younglove, B.A., J.F. Ely. Thermophysical properties of fluids. II. Methane, ethane, propane, isobutane, and normal butane, *J. Phys. Chem. Ref. Data*, 16, 4 (1987), pp. 577–798.

Zabrodsky, V.G., T.V. Lokotosh. A basic state and collective excitations in proton ordered phase of cubic ice, *Ukr. Fiz. Zh.*, 38 (1993), pp. 1714–1723.

Zallen, R. *The Physics of Amorphous Solids*. New York, NY: John Wiley and Sons (1983).

Zhuang, Z.Q., M.J. Haun, S.-J. Jang, L.E. Cross. *Ultrasonics, Ferroelectrics, and Frequency Control, IEEE Transactions on*, 36(4) (1989), p. 413.

Zolotov, M.Y., J. Kargel. *On the Chemical Composition of Europa's Icy Shell, Ocean, and Underlying Rocks*. Europa: University of Arizona Press (2009), pp. 431–458.